Biomaterials 322 (2025) 123352

Contents lists available at ScienceDirect

Biomaterials

journal homepage: www.elsevier.com/locate/biomaterials

Vascular endothelial growth factor (VEGF) and endogenous calcium-capturing gelatin methacrylate hydrogels promote bone tissue regeneration

Zhengchao Yuan [a,b,1], Xinyi Wang [a,1], Peng Li [c,1], Muhammad Shafiq [d], Panpan Shang [e], Lu Han [a], Hao Feng [a], Yuan Xu [f], Mohamed El-Newehy [g], Meera Moydeen Abdulhameed [g], Lianyong Jiang [h,*], Xiumei Mo [a,e,**], Yijiu Ren [b,***]

[a] State Key Laboratory for Modification of Chemical Fibers and Polymer Materials, Shanghai Engineering Research Center of Nano-Biomaterials and Regenerative Medicine, College of Biological Science and Medical Engineering, Donghua University, Shanghai, China
[b] Department of Thoracic Surgery, Shanghai Pulmonary Hospital, Tongji University School of Medicine, Shanghai, China
[c] Department of Orthopedic Trauma, Binzhou Medical University Hospital, Binzhou, Shandong, China
[d] Innovation Center of NanoMedicine (iCONM), Kawasaki Institute of Industrial Promotion (KIIP), Kawasaki, Japan
[e] Institute of Biomaterials and Biomedicine, School of Food and Pharmacy, Shanghai Zhongqiao Vocational and Technical University, Shanghai, China
[f] Department of Orthopaedics, Xinqiao Hospital, Army Military Medical University, No. 183, Xinqiao Street, Shapingba District, Chongqing, China
[g] Department of Chemistry, College of Science, King Saud University, P.O. Box 2455, Riyadh, Saudi Arabia
[h] Department of Cardiothoracic Surgery, Xinhua Hospital Affiliated to Shanghai Jiao Tong University School of Medicine, Shanghai, China

ARTICLE INFO

Keywords:
Peptides
Nanofiber
Hydrogel
VEGF
Bone regeneration
Electrospinning

ABSTRACT

The regeneration of irregular-shaped bone defects remains a perpetuating challenge. Scaffolds with osteogenesis and angiogenesis dual capabilities hold considerable promise for bone tissue repair. The objective of this study was to delineate the synergistic effect of calcium ions (Ca^{2+})-recruiting peptide (FVDVT, abbreviated as CP) and vascular endothelial growth factor (VEGF)-binding prominin-1-derived peptide (DRVQRQTTTVVA, abbreviated as BP) in gelatin methacrylate (GM)-based hydrogels (GM@BCP). BP-loaded hydrogels can recruit VEGF *in situ* to promote angiogenesis, as well as promote cell viability and growth as revealed by the whole transcriptome RNA sequencing of human umbilical vein endothelial cells (HUVECs). PLA/G@CP short fibers can induce bone matrix mineralization and regulate mechanical behavior of hydrogels. The GM@BCP hydrogels were found to be cytocompatible, non-toxic, and bioresorbable, as well as fill an irregular-shaped bone defect *in vivo*. Moreover, evaluation in a rat calverial defect model manifested significant promise of GM@BCP hydrogels to promote bone tissue repair by simultaneously inducing osteogenesis and angiogenesis 8 weeks post-operatively. Taken together, our approach of simultaneously harnessing *in situ* calcium ion (Ca^{2+}) binding and VEGF recruitment may have broad implications for fracture repair and potentially other related disciplines.

1. Introduction

There is an ongoing demand for novel alternatives for bone regeneration due to the high prevalence of bone diseases and traumatic bone fractures. While former can cause severe bone abnormalities and bone fragility, later may require the replacement of the fractured bone, which may lead to disability and may compromise the quality-of-life (QOL) of the patients [1]. Autograft are considered as gold standards for bone grafting albeit several risks, such as donor-site associated infection [2]. To address above-mentioned drawbacks, artificial tissue regeneration

* Corresponding author. Department of Cardiothoracic Surgery, Xinhua Hospital Affiliated to Shanghai Jiao Tong, University School of Medicine, 200092, Shanghai, China.
** Corresponding author. State Key Laboratory for Modification of Chemical Fibers and Polymer Materials, Shanghai Engineering Research Center of Nano-Biomaterials and Regenerative Medicine, College of Biological Science and Medical Engineering, Donghua University, 201620, Shanghai, China.
*** Corresponding author. Department of Thoracic Surgery, Shanghai Pulmonary Hospital, Tongji University School of Medicine, 200433, Shanghai, China.
E-mail addresses: jianglianyong@xinhuamed.com.cn (L. Jiang), xmm@dhu.edu.cn (X. Mo), ryjscott@tongji.edu.cn (Y. Ren).
[1] Z.Y., X. W., and P.L. are co-first authors.

https://doi.org/10.1016/j.biomaterials.2025.123352
Received 21 January 2025; Received in revised form 17 April 2025; Accepted 19 April 2025
Available online 22 April 2025

scaffold (ATRS) have been developed, such as hydrogels, bioactive glasses, and aerogels [3].

Especially, hydrogels with three-dimensional (3D) hydrophilic polymer networks as well as biocompatibility, biodegradability, and adaptable mechanical properties similar to native tissue, hold great promise for bone tissue repair [4,5]. Injectable hydrogels could form *in situ* gelation and help fill irregular-shaped bone defects in a minimally invasive manner, and can additionally deliver living cells or bioactive factors to the desired tissue sites [6,7]. Gelatin methacrylate (GM) has been actively pursued for tissue engineering (TE) applications, thanks to its biocompatibility, biodegradability, and mechanically tunability to obtain hydrogels of a range of mechanical properties [8,9]. Nevertheless, despite these advantages, GM hydrogels showed only marginal cell infiltration and they additionally lacked vasculogenic and mineralizing abilities, thereby necessitating alternative solutions to broaden the potential of GM hydrogels for bone regeneration [2,10].

Angiogenesis refers to the formation of capillary buds from pre-existing blood vessels to produce neo-vessels, which can promote the diffusion of oxygen as well as the transport of nutrients as needed to promote cell metabolism and remove the cell debris during tissue regeneration [11]. Vascular endothelial growth factor (VEGF) is a well-known pro-angiogenic cue, which can also promote the proliferation, migration, and viability of endothelial cells (ECs). Nonetheles, VEGF exhibits short half-life and poor retention and higher concentrations of VEGF my also induce detrimental side effects [12]. Consequently, localized and sustained presentation VEGF at the injury site may hold great promise for tissue regeneration. Recently, prominin-1-derived peptide (PR1P, DRVQRQTTTVVA, herein abbreviated as BP) has been shown to bind and stabilize VEGF *in situ* via interaction with VEGF receptor-2 (VEGFR-2) and neuropilin-1 (NRP-1), and promote angiogenesis (Fig. 1a) [13,14]. Consequently, the incorporation of BP into tissue-engineered scaffolds may be advantageous to promote angiogenesis.

Since bone defects require multiple overlapping healing strategies,

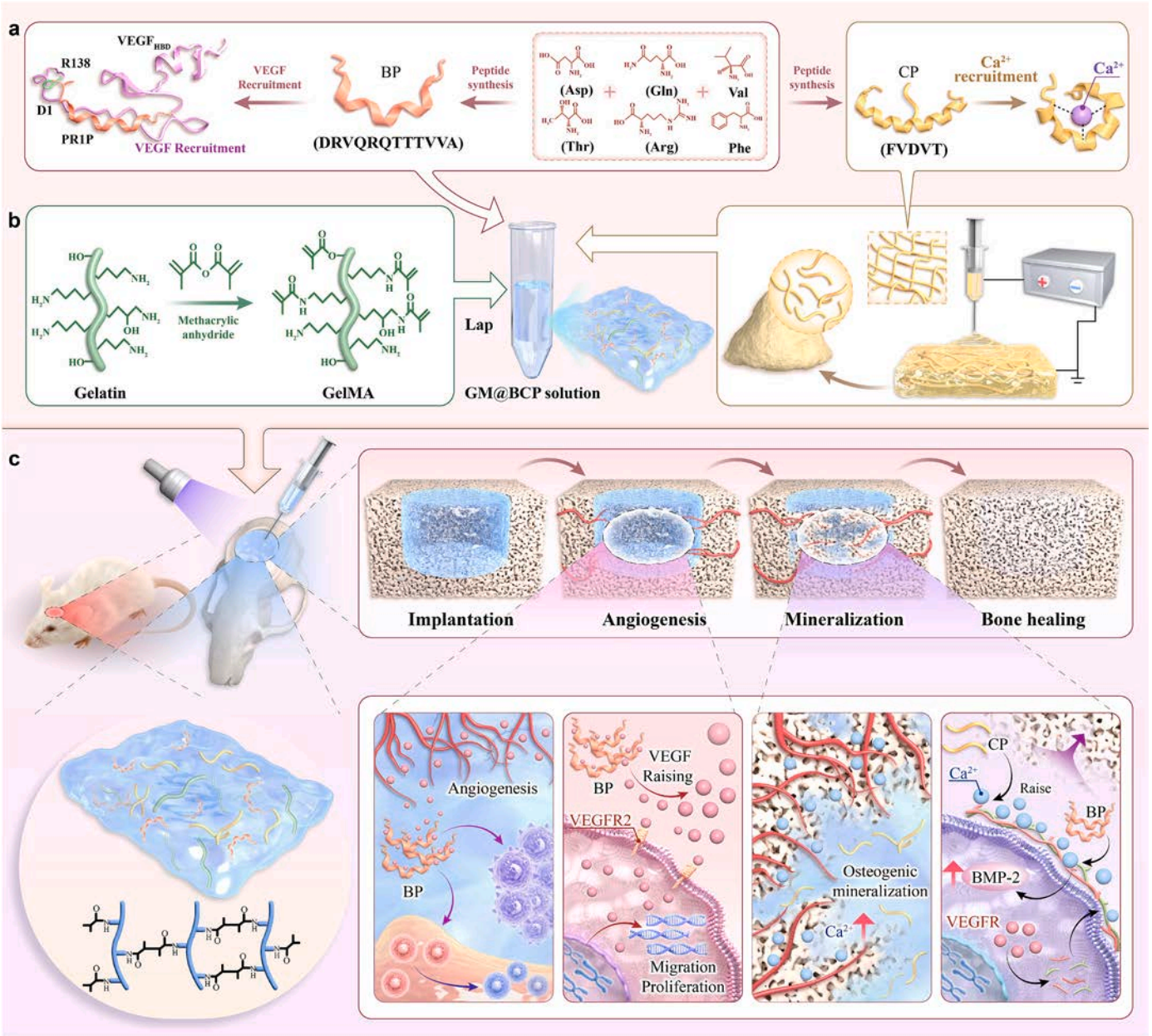

Fig. 1. An overview of the bone regeneration by the GM@BCP hydrogels. (a) The preparation of BP and CP. (b) The preparation of PLA/G@CP short fibers and GM@BCP hydrogels. (c) The healing process of GM@BCP hydrogels during bone repair.

including vasculature formation and osteogenic induction, angiogenic cues alone may not meet the requirements of high-quality bone tissue regeneration [15,16]. A novel calcium-chelating peptide (FVDVT, abbreviated as CP) from wheat germ protein hydrolysates has been shown to promote calcium binding *in situ* (Fig. 1a) [17,18]. The CP-induced recruitment of calcium ions (Ca^{2+}) may promote biomineralization and fracture healing. We anticipated that BP-mediated prior induction of vascular networks may help complement CP-mediated calcium ion (Ca^{2+}) binding to simultaneously induce angiogenesis and osteogenesis for an effective bone tissue repair.

Electrospun fibers with appropriate mechanical strength, flexibility, and eco-friendly nature may provide an amenable platform for an effective encapsulation of different types of therapeutics and biologics as needed for tissue repair [12,19]. Moreover, electrospun fibers can recapitulate the morphological features of extracellular matrix (ECM) and therefore they can leverage a conduicive environment for cell-cell and cell-material interaction [20]. Nevertheless, electrospun fibers still require further optimization, especially, for bone TE applications in terms of the required mechanical strength, porosity, pore size, and poor-interconnectiveity [21,22]. Poly(lactic acid)/gelatin (PLA/G) short fibers have been successfully used to strengthen hydrogels, which may also be exploited for the sustained and controlled release of bioactive cues for functional tissue repair [23,24]. Consequently, fiber-hydrogel-based three-dimensional (3D) tissue-engineered bone scaffolds can be engineered to sequentially release BP and CP to promote *in situ* bone tissue repair (Fig. 1b).

The objective of this study was to achieve sustained and controlled release of BP and CP to promote bone tissue repair. The BP can bind VEGF *in situ* and stabilize its concentration at the bone defect site for angiogenic induction and neo-vessel formation. On the other hand, the CP can increase the recruitment of calcium ions (Ca^{2+}), which can enhance osteogenic induction and biomineralization at injury site. To achieve different release profile of BP and CP preferential vascularization and subsequent osteogenic induction, we directly loaded BP into GM hydrogels containing CP-loaded PLA/G short fibers (PLA/G@CP) into GM hydrogels to obatin. These fiber-hydrogel scaffolds can help realize sequential recruitment of VEGF and binding of calcium ions (Ca^{2+}) *in situ*. GM@BCP hydrogels exhibited good biocompatibility, angiogenic ability, and *in situ* mineralization (Fig. 1c).

2. Experimental

2.1. Materials

Lithium phenyl-2,4,6-trimethylbenzoylphosphinate (LAP) and GelMA (GM, EFL-GM-90, DS: 90 %) were obtained from Yongqinquan Intelligent Equipment Co., Ltd., Suzhou, China. PLA (DG-L150) was purchased from Jinan Daigang Biomaterial Co., Ltd., Jinan, China. 1,1,1,3,3,3-hexafluoro-2-propanol (HFIP) was acquired from Shanghai Darui Fine Chemical Co., Ltd., Shanghai, China. Prominin-1-derived peptide (PR1P, abbreviated as BP, amino acid sequence, DRVQRQTTTVVA) and CP (amino acid sequence, FVDVT) were custom-synthesized by China Peptides Co., Ltd., Shanghai, China. Human umbilical vein endothelial cells (HUVECs) and MC-3T3-E1 (ATCC) were supplied by the Institute of Biochemistry and Cell Biology of Chinese Academy of Sciences, Shanghai, China. Rat bone-marrow mesenchymal stem cells (rBMSCs) was isolated from Sprague-Dawley (SD) rats (2-week-old) [8].

2.2. Preparation of hydrogels

2.2.1. Preparation of PLA/G@CP short fibers

To prepare PLA/G@CP short fibers, PLA and Gel (7:3, *w/w*) and CP (20 wt%) were dissolved in HFIP to obtain 10 % (w/v) PLA/G@CP solution. PLA/G@CP fibers were prepared using electrospinning (Yongkang Leye Technology Development Co., Ltd., Beijing, China, model # SS-3556H) and the fabrication conditions were as follows: needle size, 21 G, applied voltage, 10 kV, flow rate, 1.5 mL/h. PLA/G@CP fibers were dispersed in *tert*-butyl alcohol to prepare short fibers dispersions using a homogenizer followed by freeze-drying for 48 h. Since Gel can degrade rapidly, PLA and PLA@CP short fibers were additionally prepared using similar method to avoid an interference of Gel on the subsequent mineralization assay (Fig. S1, Supporting Information). The PLA and PLA @CP fiber were also prepared by the same method.

2.2.2. Preparation of GM@BCP hydrogels

To prepare hydrogels, GM and LAP was dissolved using phosphate-buffered saline (PBS) (GM, 8 %, *w/v* and LAP, 0.05 %, *w/v*) and sterilized with a 0.22 μm filter paper. The GM does not contain BP and PLA/G@CP short fibers. For GM@BP and GM@CP hydrogels, 1 mg of BP and 10 mg PLA/G@CP short fibers were added into a total 10 mL of the GM solution, respectively. On the other hand, for GM@BCP hydrogels, 1 mg of BP and 10 mg of PLA/G@CP short fibers were added into GM/LAP solution. For crosslinking, hydrogel solutions were poured into respective molds and cross-linked by blue light (wavelength, 405 nm).

2.3. Physicochemical analysis

To elucidate the ability of the CP to induce mineralization as well as discern physical and chemical properties of hydrogels, Alizarin Red S (ARS) staining was performed. Moreover, the recruitment of calciukm ions (Ca^{2+}) as well as mechanical properties, and degradation of hydrogels were studied. The detailed methods are provided in Supplementary Information.

2.4. Biocompatibility and biological functions of scaffolds in vitro

The biocompatibility and biological functions of hydrogels were studied with different types of assays, including live/dead staining, cell proliferation assay, Transwell migration assay, scratch wound healing assay, tube formation, alkaline phosphatase assay (ALP) activity, ARS staining, expression of bone morphogenetic protein-2 (BMP-2) and collagen type I (Col-I) in bone marrow mesenchymal stem cells (BMSCs) were carried out *in vitro*. We additionally performed transcriptome analysis of untreated as well as BP-treated HUVECs. The detailed methods are provided in Supplementary Information.

2.5. Animal experiments

All *in vivo* experiments were approved by the Institutional Animal Care and Use Committee (IACUC) of the Army Military Medical University (AMUWEC20235045).

2.5.1. Biocompatibility in vivo

To elucidate the biocompatibility of hydrogels *in vivo*, hydrogel solution was prepared into a slice shape ($\varphi = 10$ mm; thickness = 2 mm). 4-week-old Sprague-Dawley (SD) rats were anesthetized with an intraperitoneal injection of pentobarbital sodium (60 mg/mL). The skin was shaved and subcutaneous pocket was created. Hydrogels were subcutaneously transplanted in animals for up to 4 weeks ($n = 3$). At 2, 3, 4 weeks post-operatively, hydrogels alongside adjacent tissues were explanted, fixed, paraffin-embedded, sectioned, and subjected to hematoxylin and eosin (H&E) staining and Masson's trichrome (MT) staining.

The chronic toxicity assay was carried out to discern the long-term cytotoxicity and immunological response of the degradation byproducts of hydrogel *in vivo*. The 20 ICR rat (6-week-old; male) were randomly divided into 4 groups, including GM, GM@BP, GM@CP, and GM@BCP. Approximately, 200 μL of hydrogel solution was subcutaneously injected into rats for up to 30 days ($n = 5$). At day 0, 3, 5, 9, 15, 20, 30, the weight of rats was measured. Main organs, including heart, liver, spleen, lung, and kidney were retrieved and subjected to H&E staining.

On the other hand, the blood was collected from the eyeball for routine blood analysis (*e.g.*, white blood cell, WBC; neutrophils, Neu; lymphocytes, Lym; monocytes, Mon; red blood cells, RBC; hemoglobin, HGB; platelets, PLT, etc.) and serum biochemical analysis (*e.g.*, alanine aminotransferase, ALT; Aspartate transaminase, AST; Blood urea nitrogen, BUN; Creatinine, CREA; Urea, UA, etc.) at day 30.

2.5.2. Bone regeneration in vivo

SD rats (male, 6 weeks-old, $n = 12$) were anesthetized by intraperitoneal injection of pentobarbital sodium (60 mg/kg). Calverial defects (thickness, 5 mm) were established. Bone debris was cleaned, and different types of hydrogel solutions, such as GM, GM@BP, GM@CP, and GM@BCP were injected into the bone defect site followed by light irradiation (wavelength, 405 nm) for 40 s ($n = 3$). Defects without hydrogel were used as a control group. SD rats were euthanized and calvarial were harvested 8 weeks post-operatively. For bone regeneration, harvested calvaria was fixed with paraformaldehyde (PFA) and analyzed with microcomputed tomography (micro-CT). Thereafter, harvested tissues were decalcified, paraffin-embedded, sectioned, and subjected to H&E and MT staining as well as immunofluorescent (IF)

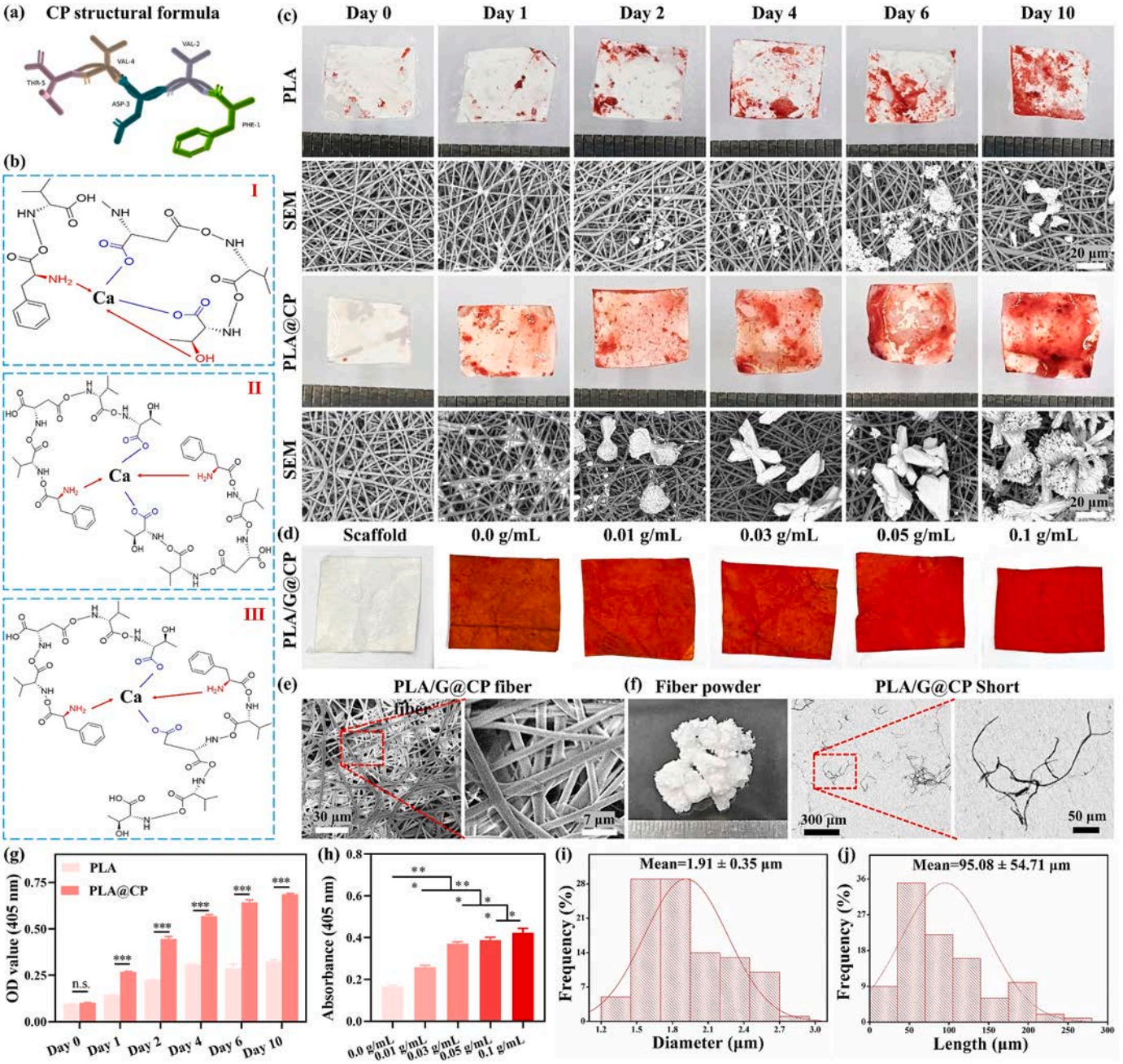

Fig. 2. Characterization of PLA/G@CP fiber. (a) Structural formula of CP. (b) Schematic illustration of the chelation of calcium ions (Ca^{2+}) with CP. (c) ARS staining and SEM micrographs to elucidate mineralization of fibers incubated along with the SBF for up to different time points *in vitro*. The colour intensity of the ARS as well as deposition of inorganic minerals was distinct in PLA@CP fibers than that of the PLA fibers, which were further increased with an increase in the incubation time. (d) ARS staining of PLA/G@CP treated with different concentrations of calcium chloride ($CaCl_2$) for up to 24 h. SEM micrographs of PLA/G@CP fiber (e), optical photograph and SEM micrographs of PLA/G@CP short fiber (f). Quantitative analysis of ARS staining for mineralization in SBF (g), and PLA/G@CP treated with different concentrations of calcium chloride ($CaCl_2$) (h). The mean diameter of PLA/G@CP fiber (i) and the mean length of PLA/G@CP short fiber (j). (For interpretation of the references to colour in this figure legend, the reader is referred to the Web version of this article.)

staining. Detailed preparation process as well as the staining of harvested tissue sections is described in Supporting Information.

3. Results

3.1. Preparation and characterization of hydrogels

The CP is composed of five amino-acids (FVDVT), which can chelate calcium ions (Ca^{2+}) (Fig. 2). The predicted structure of CP is shown in Fig. 2a. It has been previously shown that the CP can chelate calcium ions (Ca^{2+}) via two carboxylic (-COOH) groups, one amino (-NH_2) group, and one hydroxyl (-OH) group (Fig. 2b). Moreover, two CP sequences can form two types of complexes to chelate calcium ions (Ca^{2+}). CP-Ca complex is formed with two amino (-NH_2) groups and two carboxylic (-COOH) groups from two CP molecules (Fig. 2b) [17]. The CP was loaded into PLA/G fibers to obtain PLA/G@CP fiber. The incorporation of CP into PLA fibers is expected to increase the concentration of calcium ions (Ca^{2+}) around the fiber, thereby facilitating the mineralization of simulated body fluid (SBF). SEM micrographs exhibited distinct inorganic minerals surrounding PLA/G@CP fibers after incubation in the SBF (Fig. 2c). Moreover, fibers exhibited positive staining for ARS. The colour intensity of ARS staining was increased with an increase in the incubation time of the PLA/G@CP in the SBF than that of the PLA group (Fig. 2c and g).

ARS staining of PLA/G@CP fibers treated with different concentrations of calcium chloride ($CaCl_2$) exhibited that the binding of the calcium ions (Ca^{2+}) was steadily increased with an increase in the content of calcium chloride ($CaCl_2$) (Fig. 2d). The intensity of ARS staining was also gradually increased with an increase in the concentration of calcium chloride ($CaCl_2$) (Fig. 2d). The absorbance of the supernatant was measured (OD value, 450 nm) and was found to be 0.17 ± 0.01, 0.26 ± 0.01, 0.37 ± 0.01, 0.39 ± 0.01, and 0.42 ± 0.02 for 0.0, 0.01, 0.03, 0.05, and 0.1 g/mL of calcium chloride ($CaCl_2$) solution for (Fig. 2h).

PLA/G@CP showed continuous fibrous structure, which were then converted into short fibers of varying lengths through homogenization (Fig. 2e and f). Average diameter and average length of PLA/G@CP short fibers were 1.91 ± 0.35 μm and 95.08 ± 54.71 μm, respectively (Fig. 2i and j). The GM, as a widely applied photo-cross-linked hydrogel,

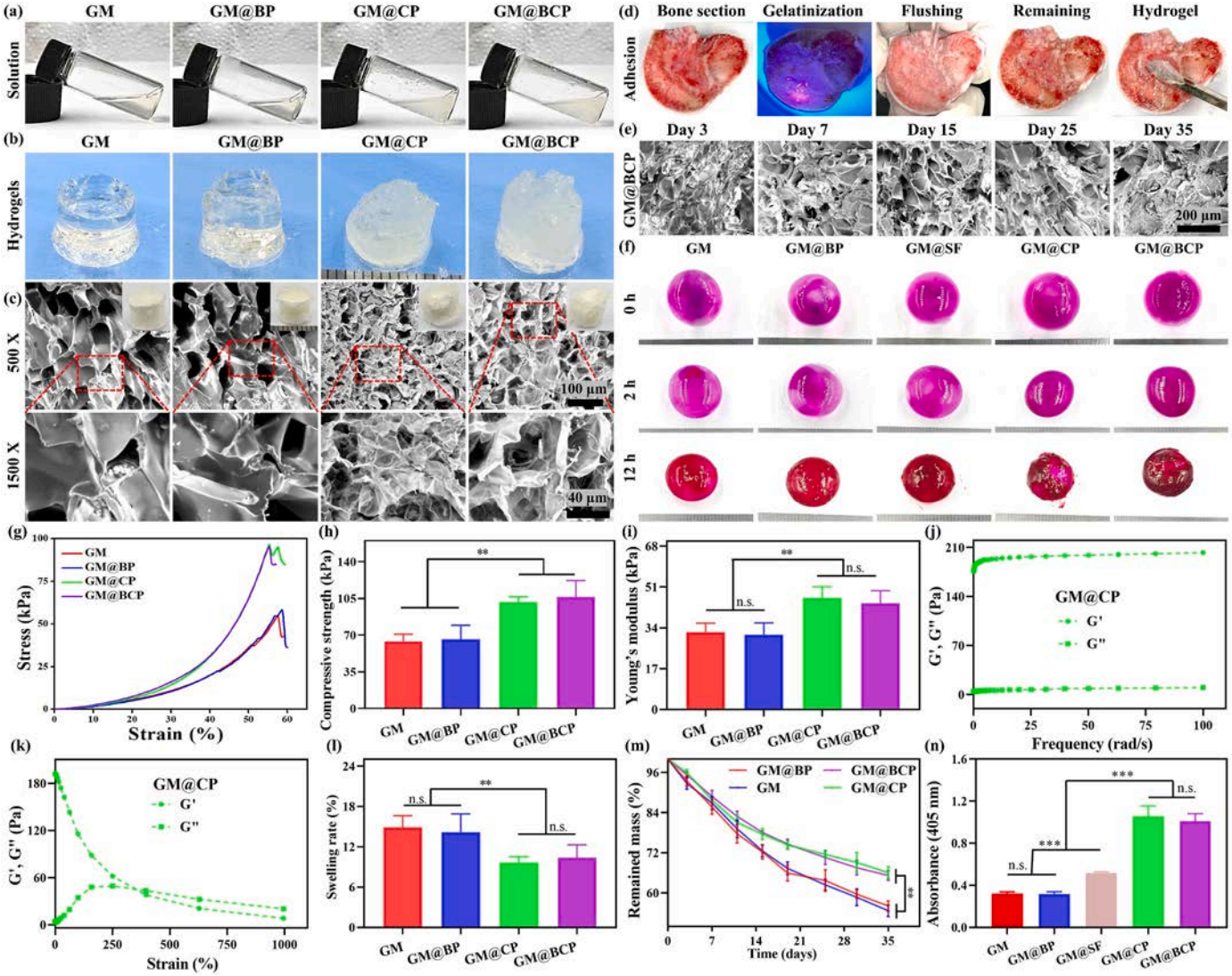

Fig. 3. Characterization of hydrogels. (a) Optical photographs of different types of hydrogels. (b) The appearance of hydrogel. (c) SEM micrographs of freeze-dried hydrogels at different magnifications. (d) Adhesion of GM@BCP hydrogels with tissues. (e) Morphological analysis of GM@BCP hydrogels after degradation for up to day 35 *in vitro*. The degraded hydrogels were freeze-dried for SEM imaging. (f) ARS staining of different types of hydrogels for mineralization with SBF for up to different time points *in vitro*. Representative compressive stress-strain curves of various hydrogels (g), maximum compressive strength (h), and Young's modulus (i). Rheological analysis of hydrogels (j), strain sweep analysis of GM@CP hydrogels (k). Swelling rate (l) and residual weight (m) for hydrogels after degradation for up to different time points *in vitro*. Quantitative analysis of ARS staining of hydrogels mineralized with SBF *in vitro* (n).

was found to be transparent and colorless (Fig. 3a). On the other hand, the BP is composed of 12 amino acids, which may not alter the physical properties of the GM hydrogel (Fig. 3b). The addition of PLA/G@CP sort fibers turned GM hydrogels into turbid without precluding the photo-crosslinking ability. As shown in Fig. 3b, the GM and GM@BP hydrogels were colorless and transparent, while GM@CP and GM@BCP hydrogels appeared to be white and opaque. There was an insignificant difference among dry hydrogels in term of the physical appearance. SEM images of dry GM@CP and GM@BCP hydrogels exhibited smaller pore size and a random distribution of short fibers than that of GM and GM@BP hydrogels (Fig. 3c).

We next discerned the adhesion behavior of GM@BCP hydrogels to elucidate their ability to fill irregular-shaped bone defects. The GM@BCP hydrogels were strongly bound to the defect (Fig. 3d). All hydrogel groups exhibited similar compressive stress-strain curves (Fig. 3g). The compressive modulus was found to be 32.3 ± 3.7 kPa, 31.3 ± 4.8 kPa, 46.5 ± 4.6 kPa, and 44.3 ± 5.1 kPa, while maximum compressive strength was found to be 64.2 ± 6.8 kPa, 65.9 ± 13.5 kPa, 101.7 ± 5.0 kPa, and 106.5 ± 15.7 kPa for GM, GM@BP, GM@CP, and GM@BCP hydrogels, respectively (Fig. 3h and i). These results manifested that the incorporation of BP into the hydrogels did not adversely influence mechanical properties. On the other hand, the incorporation of PLA/G@CP short fiber into hydrogels can significantly improve the compressive mechanical properties of hydrogels. Rheological analysis also mirrored compressive mechanical analysis; the incorporation of PLA/G@CP into hydrogels led to significant promotion in the mechanical performance (Fig. 3j and k & Fig. S2, Supporting Information).

We further evaluated the swelling of the hydrogels. While hydrogels exhibited noticeable swelling, there was an insignificant difference in the hydrogel shape even after swelling (Fig. S3, Supporting Materials). All hydrogels attained maximum swelling within 24 h. The values for the percentage swelling were found to be 14.2 ± 2.7 %, 12.5 ± 6.1 %, 9.7 ± 0.9 %, 10.4 ± 2.0 % for GM, GM@BP, GM@CP, and GM@BCP groups, respectively (Fig. 3l). The shape of the hydrogels began distorting at 48 h, which may be ascribed to the hydrogel degradation (Fig. S4, Supporting Materials). All hydrogels were degraded over time. GM@CP and GM@BCP hydrogels exhibited distinct fiber morphology upon degradation presumably owing to the slower degradation of PLA/G@CP short fibers (Fig. 3e & Fig. S5, Supporting Materials). The residual weight percentage of the hydrogels was 56.1 ± 1.6 %, 54.7 ± 1.7 %, 66.1 ± 1.8 %, and 65.3 ± 1.5 % for GM, GM@BP, GM@CP and GM@BCP groups at day 35, respectively as compared to the weight of the hydrogels at day 0 (Fig. 3m).

The GM@BCP hydrogels should retain photo-crosslinking characteristics upon *in situ* transplantation (Fig. S6a, Supporting Materials). As can be seen from Fig. S6b–c (Supporting Materials), PLA/G@CP short fiber can reduce the fluidity of the solution, while the BP had only a little effect on the injectability resistance of the solution. The viscosity was found to be 0.1 Pa s, 3188.4 Pa s, 16184.7 Pa s, and 15617.2 Pa s at 0.001 1/s; 0.1 Pa s, 8.1 Pa s, 11.3 Pa s, and 76.0 Pa s at 1 1/s; and 0.01 Pa s, 0.01 Pa s, 0.01 Pa s, and 0.04 Pa s at 100 1/s for water, GM, GM@CP, and GM@BCP groups, respectively. These results showed that the incorporation of short fibers can increase the viscosity of hydrogels in the low shear rate range (Fig. S7, Supporting Materials). To further ascertain the homogenous fluidity and potentially injectability, we printed a letter *"DHU"* with GM@BCP hydrogel (Fig. S8, Supporting Materials).

To delineate the mineralization potential of hydrogels, we carried out ARS staining *in vitro*. Hydrogels appeared to be of purple red colour even at $t = 0$ h presumably owing to the adsorption of the dye (Fig. 3f & Fig. S9(a–b), Supporting Materials). By 12 h, GM@SF, GM@CP, and GM@BCP hydrogels exhibited intense red mineralized layers (Fig. S9a and 9c, Supporting Materials). Quantitative analysis showed an absorbance value of 0.34 ± 0.05, 0.32 ± 0.02, 0.52 ± 0.01, 1.06 ± 0.10, and 1.01 ± 0.07 for GM, GM@BP, GM@SF, GM@CP, and GM@BCP hydrogels, respectively (Fig. 3n). By 24 h, the colour intensity of the mineralized layer was further increased. Moreover, the absorbance values were significantly higher at $t = 24$ h than that of the absorbance values at $t = 12$ h (0.98 ± 0.27, 1.11 ± 0.05, 1.36 ± 0.03, 1.87 ± 0.07, 1.88 ± 0.02 for GM, GM@BP, GM@SF, GM@CP, and GM@BCP groups, respectively at 24 h (Fig. S9d). Therefore, these data showed that the CP can promote mineralization, but also increase the total amount of mineralization, indicating the potential of the hydrogels to promote mineralization *in vitro*.

Since we incorporated BP and CP into hydrogels for the binding and stabilization of VEGF to promote angiogenesis as well as the recruitment of calcium ions (Ca^{2+}) *in situ* to induce mineralization, the release kinetics of BP and CP may be of considerable significance. We used Fluorescein-5-isothiocyanate (5-FITC) and Rhodamine B to respectively discern the release kinetics of CP and BP, *in vitro*. While Rhodamine B exhibited rapid release at the initial time points, it displayed sustained release for up to 18 days *in vitro*. In contrast, 5-FITC was slowly released within the first 12 days followed by its rapid release from day 15 onwards (Fig. S10, Supporting Materials). These results showed that the BP and CP can be released in a sustained and controlled fashion, which is ascribed to their incorporation into different carriers.

3.2. Biocompatibility and biological functions of scaffolds in vitro

We next deciphered the cytocompatibility of scaffold using HUVECs and BMSCs (Fig. 4) [25]. We used HUVECs due to their pivotal role in angiogenesis and BMSCs due to their ability to promote biomineralization via differentiation into osteoblasts as well as the production of the ECM (Fig. 4a) [16]. As shown in Fig. 4b, BMSCs and HUVECs were seeded on the surface of hydrogels for up to 5 days, which displayed good viability (see green and red colour for live and dead cells, respectively). Cell proliferation by cell counting kit-8 (CCK-8) assay also displayed the proliferation of both cell types (Fig. 4f and g). These results indicated that the incorporation of BP and PLA/G@CP short fibers into GM hydrogels did not adversely influence the cytocompatibility of hydrogels. It is worth ot note that the hydrogels exhibited lower OD values than that of the control group (cell cultured along with the medium alsone) presumably due to an uneven surface of hydrogel as well as certain degree of swelling and degradation of the hydrogels during cell culture, which may suppress cell adhesion and spreading (Fig. 4f and g).

Cell migration was studied by scratch wound healing assay and Transwell migration assay (Fig. 4a). GM@BP and GM@BCP hydrogels exhibited significantly higher migration of BMSCs and HUVECs than that of the control, GM, and GM@CP hydrogels (Fig. 4c). Quantitative analysis further mirrored the quantitative results; GM@BP and GM@BCP hydrogels outperformed other groups in terms of the number of the migrated cells (Fig. 4h). Scratch wound healing assay also showed significantly more migration of HUVECs (Fig. 4d). HUVECs treated with the extract solution of GM@BP and GM@BCP exhibited considerably higher migration as compared to the other groups (Fig. 4i). These results showed that the incorporation of BP into the hydrogels led to more cell migration.

The BP can promote angiogenesis by binding VEGF *in situ* as well as enhancing its stability. To elucidate the ability of the BP-laden hydrogels to promote angiogenesis, we carried out tube formation assay of HUVECs *in vitro* (Fig. 4e) [26]. HUVECs treated with the extract solution of GM@BP and GM@BCP hydrogels displayed the formation of distinct vessel-like structures. Quantitative analysis of angiogenic parameters exhibited significantly more number of nodes in GM@BCP hydrogels in comparison to the PBS (control group) as well as GM and GM@CP groups (Fig. 4j). Therefore, these results revealed that the incorporation of BP may be conducive to promote angiogenesis.

The osteogenesis of BMSCs was next elucidated after their induction in osteogenic medium for up to 14 days *in vitro* (Fig. 5). As can be seen in Fig. 5b and c, osteogenically-induced BMSCs exhibited a well-spread morphology in all groups. GM@BP, GM@CP, and GM@BCP groups displayed higher fluorescence intensity of BMP-2 than that of other

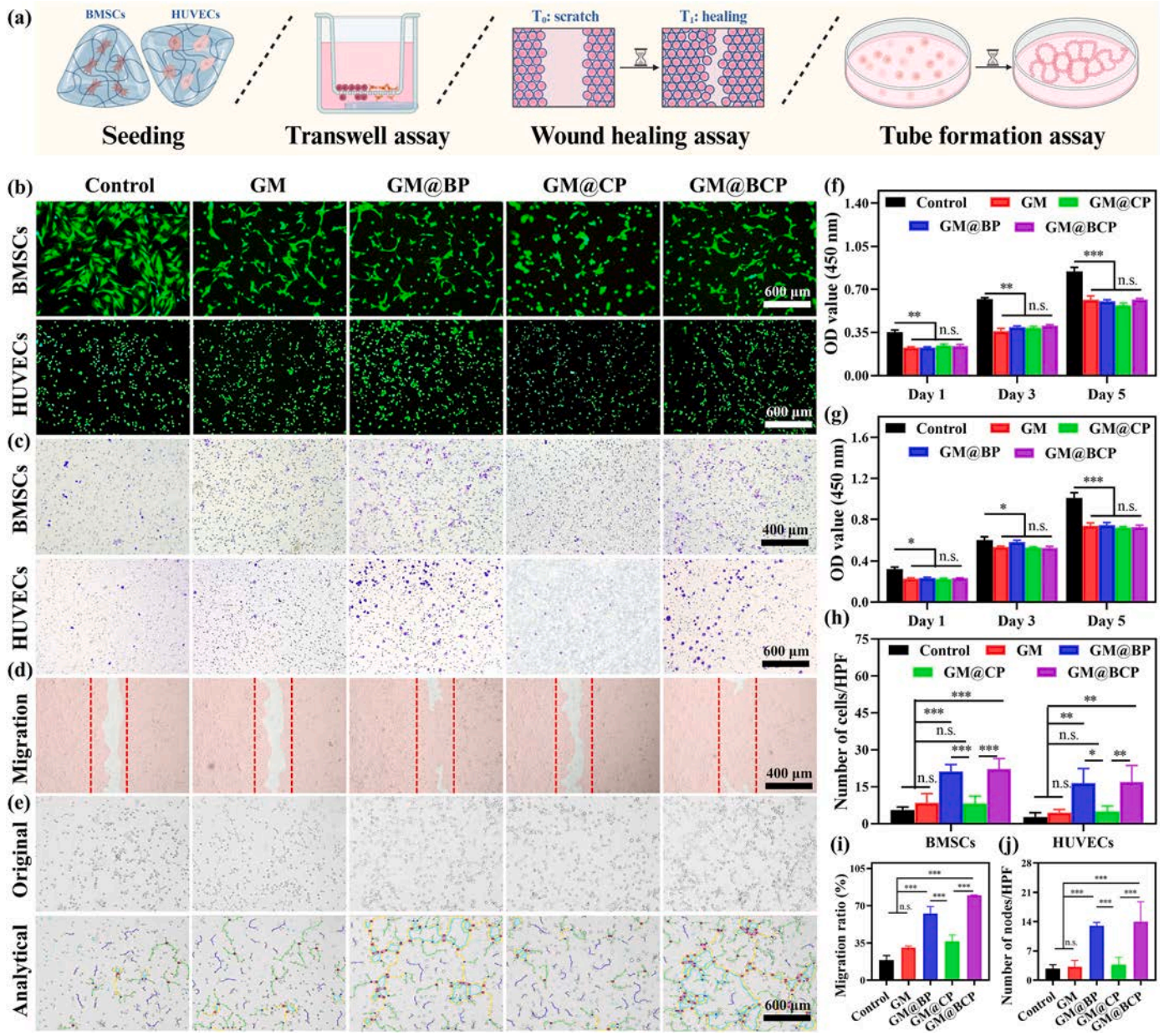

Fig. 4. Biocompatibility and biofunction of hydrogels *in vitro*. (a) Schematic illustration of biocompatibility and biofunction assay of hydrogels. (b) Live/dead staining of BMSCs and HUVECs seeded in different types of hydrogels at day 5. (c) Migration of BMSCs and HUVECs in a Transwell migration assay *in vitro*. (d) Scratch wound healing assay of HUVECs at 24 h. (e) Tube-formation assay of HUVECs at 6 h. Proliferation of rBMSCs (f) and HUVECs (g). (h) The number of recruited BMSCs and HUVECs in a Transwell migration assay. The migration ratio in the scratch wound healing assay (i), and the number of nodes in the tube-formation assay (j).

groups; the GM@CP and GM@BCP groups outperformed other groups in terms of the fluorescence intensity of BMP-2 (Fig. 5b and f). GM@BP and GM@BCP groups also exhibited higher fluorescence intensity of Col-I in comparison with the other groups (Fig. 5c and g). These results showed the beneficial effect of GM@BCP hydrogels to promote BMSCs osteogenesis, which may be attributed to the synergistic effect of BP and PLA/G@CP short fibers to promote the synthesis of BMP-2 and Col-I.

We further utilized MC-3T3-E1 and BMSCs for osteogenic induction and performed ARS staining to analyze calcium deposition at day 14. As shown in Fig. 5d and e, GM@CP and GM@BCP groups exhibit distinct red color and significantly higher mineralization degree compared with other groups. Quantitative analysis of ARS staining also manifested mineralization promoting effect of GM@CP and GM@BCP groups due in part to the osteogenic ability of PLA/G@CP short fibers (Fig. 5h and i). ALP staining also showed distinct enzyme activity in the GM@BP, GM@CP, and GM@BCP groups than that of the GM group; GM@BCP group outperformed other groups in terms of the ALP activity (Fig. 5e). These results showed advantageous effect of BP and PLA/G@CP to promote osteogenesis, which may also have implications to promote bone tissue repair *in vivo*.

To explore molecular mechanisms of BP-mediated HUVECs' angiogenesis, we carried out whole transcriptome RNA sequencing (Fig. 6). HUVECs treated with PBS were used as a control group. The PCA results showed differential RNA expression between BP and TCP groups while volcano plots showed 3746 upregulated genes and 996 downregulated genes in the BP group than that of the TCP group (Fig. 6a–b, 6d). Gene genome circle map also showed sufficient expression of differentially expressed genes (Fig. 6c).

KEGG enrichment analysis displayed significant upregulated gene expression differences between BP and TCP groups, including transfer

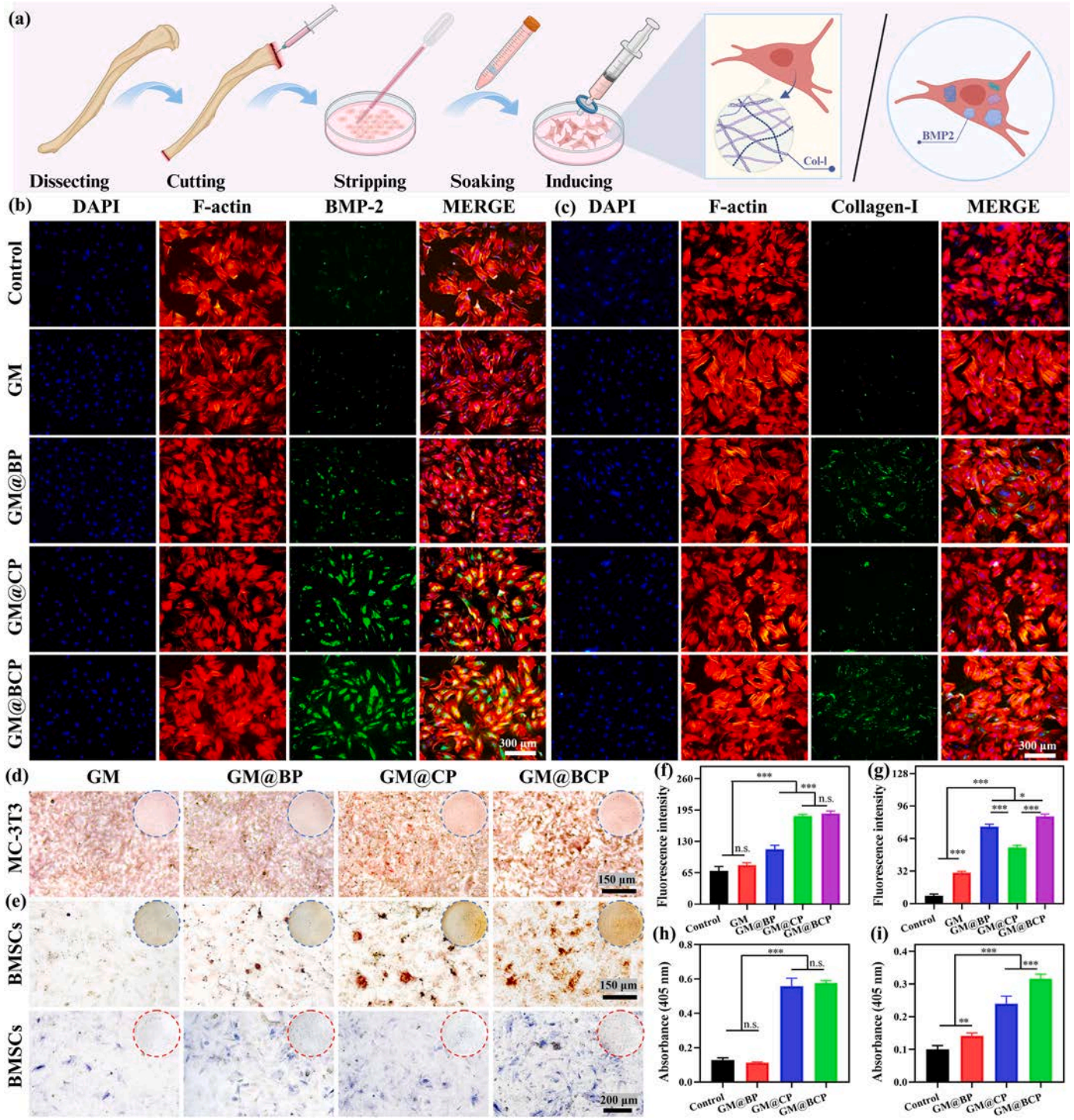

Fig. 5. Osteogenic ability of different types of hydrogels. (a) Schematic illustration of osteogenesis assay *in vitro*. (b, c) Osteogenic induction of BMSCs for up to 14 days *in vitro*. Cells were stained with F-actin (red), DAPI (blue), and BMP-2 (green). Moreover, cells were stained with F-actin (red) and Col I (green). (d) ARS staining of MC-3T3-E1 at day 14. (e) ALP and ARS staining of osteogenically-induced BMSCs at day 14. Fluorescence intensity of BMP-2 (f) and Col-I (g) acquired from immunofluorescence (IF) staining of osteogenically-induced BMSCs. Quantitative analysis of ARS staining of MC-3T3-E1 (h) and BMSCs (i). (For interpretation of the references to colour in this figure legend, the reader is referred to the Web version of this article.)

RNA (tRNA) biogenesis, messenger RNA (mRNA) biogenesis, transcription factors, mismatch repair, protein export, protein kinases as well as various signaling pathways (Fig. 6e).

On the other hand, differential downregulated gene expression between in BP *vs.* TCP groups for KEGG enrichment analysis were related to metabolism and growth regulation, such as Ras signaling pathway, estrogen signaling pathway, arachidonic acid metabolism, glycerophospholipid metabolism, sulfur metabolism and so on (Fig. S11a, Supporting Materials). The difference between BP *vs.* TCP groups in terms of the downregulated gene expression for GO enrichment analysis were focused on cell differentiation and autophagy regulation, including fat cell differentiation, negative regulation of cell growth, negative regulation of EC differentiation, apoptotic process, and positive regulation of T cell apoptotic process and so on (Fig. S11b,

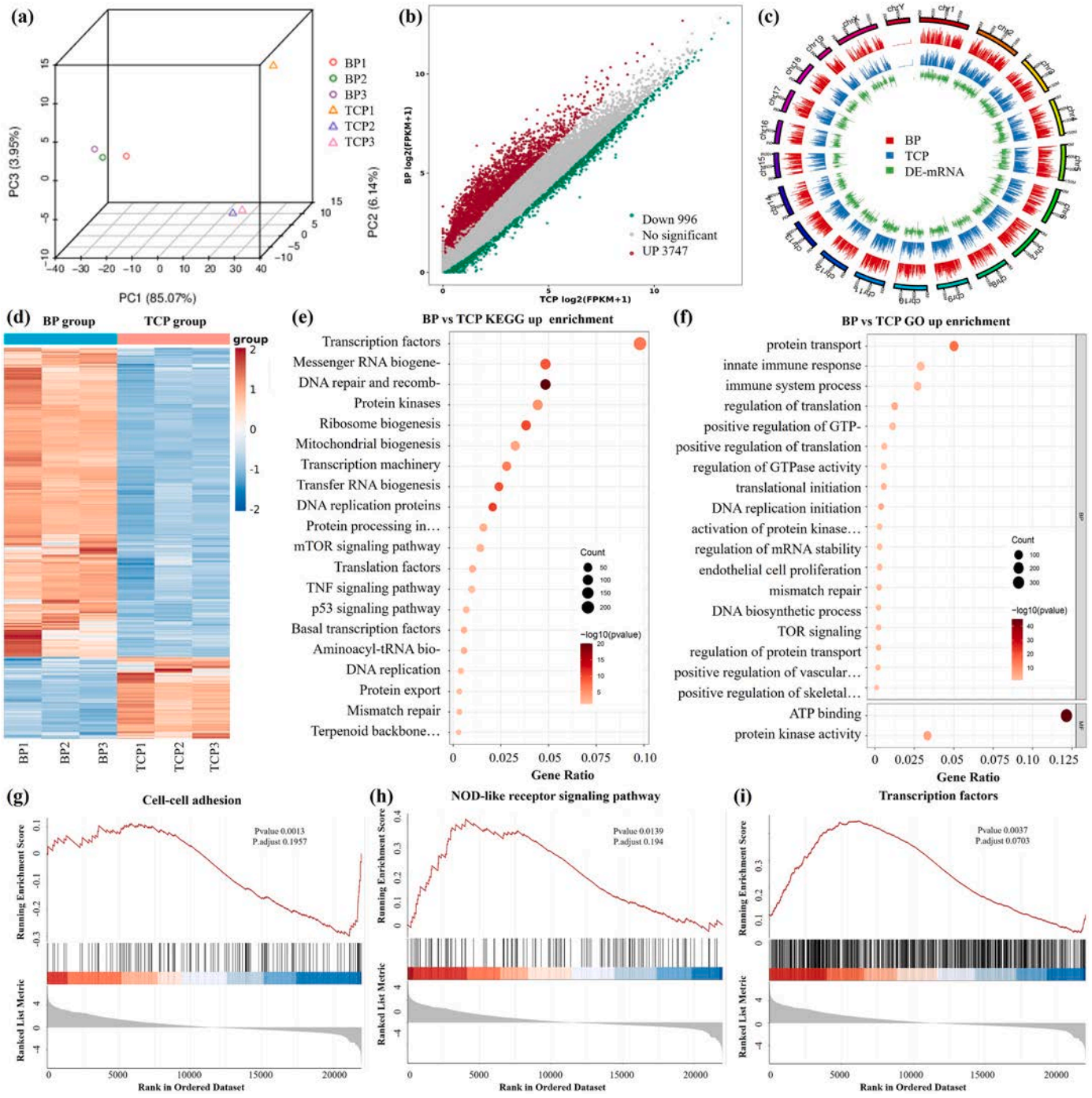

Fig. 6. Mechanisms of BP-modulated HUVECs. (a) Principal component analysis (PCA) of BP and TCP groups. (b) Volcano map of differential genes between BP and TCP groups. (c) Differential gene genome circle map of BP and TCP groups. (d) Heat map of differential genes between BP and TCP groups. KEGG pathway enrichment analysis (e), and GO enrichment analysis (f) of the upregulated genes. (g–i) GSEA enrichment analysis of cell-cell adhesion, NOD-like receptor signaling pathway, and transcription factors. *p < 0.05, **p < 0.01, and ***p < 0.001.

Supporting Materials). Gene set enrichment analysis (GSEA) showed an upregulation of cell-cell adhesion and transcription factors, as well as downregulation of the NOD-like receptor signaling pathway, which were consistent with the KEGG and GO enrichment analysis results (Fig. 6g–i). Taken together, these results showed an advantageous effect of BP in terms of cell viability, cell proliferation, and inflammation resolution via regulation of key gene transcription.

3.3. Biocompatibility in vivo

To discern biocompatibility of hydrogels as well as degradation behavior of BP and PLA/G@CP on hydrogels *in vivo*, GM, GM@BP, GM@CP, and GM@BCP hydrogels were subcutaneously implanted into SD rats for up to 28 days (Fig. 7). As shown in Fig. 7b, all hydrogels had gradually degraded over time *in vivo*. Particularly, cell infiltration was more obvious in GM@BP hydrogels in comparison to the other groups at day 14 post-operatively (Fig. 7b). H&E staining of explanted hydrogels showed visible fibers in GM@CP and GM@BCP groups, which is

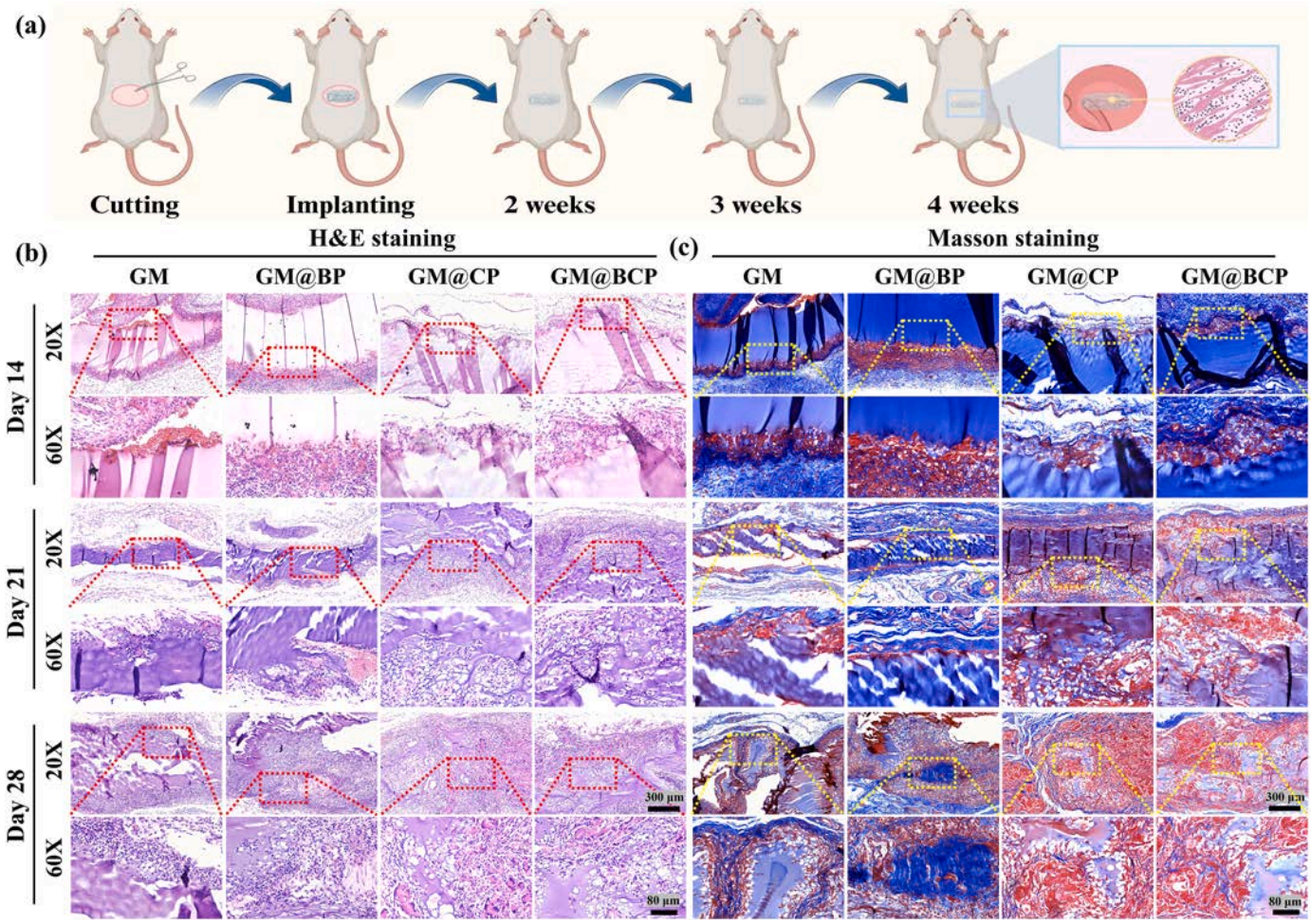

Fig. 7. Subcutaneous implantation of hydrogel in rats. (a) Schematic representation of biocompatibility assay of hydrogel for 28 days. At day 14, 21, and 28, explants as well as surrounding tissues were harvested and subjected to hematoxylin and eosin (H&E) staining (b) and Masson's trichrome staining (c).

indicative of the residual PLA/G@CP short fibers; these fibers can prolong hydrogel degradation (Fig. 7b). By day 28, the GM group was shown to be intact, while other groups exhibited infiltration of large number of host cells, thereby indicating an obvious degradation of the hydrogels. MT staining showed that all hydrogels were gradually replaced by neo-tissues alongside collagen deposition (Fig. 7c).

For long-term cytotoxicity and immunological response to the degradation byproducts of the subcutaneously implanted hydrogels, hydrogels were injected into the ICR rats for up to 30 days (Fig. 8). As shown in Fig. 8a and b, main organs, including heart, liver, lung, spleen, and kidney did not show distinct lesions, such as tissue necrosis and edema formation. The body weight of all rats was increased in all groups for up to day 9 albeit an insignificant difference among groups (Fig. 8c). The weight of hydrogels was increased even further as implantation time progressed and was found to be 13.9 ± 0.8 mg, 13.2 ± 0.8 mg, 13.4 ± 0.9 mg, 13.9 ± 1.0 mg, and 13.8 ± 1.0 mg for GM, GM@BP, GM@SF, GM@CP, and GM@BCP groups at day 30, respectively (Fig. 8d). Routine blood analysis further revealed an insignificant change in the number of blood cells (Lym, Mon, Neu, PLT, WBC, RBC) as well as hemoglobin content (HGB), which were all within the normal range (Fig. 8e–k). Serum biochemical analysis showed that the content of UA, BUN, CREA, ALT, and AST were all within normal ranges, which is indicative of the safety of hydrogels toward kidney and liver (Fig. 8l–p).

3.4. Bone regeneration in vivo

Osteo-inductive ability of hydrogels was evaluated in a rat calverial defect model for up to 8 weeks (Fig. 9 & Fig. S12, Supporting Materials). Micro-CT images showed *de novo* bone production in GM@BP, GM@CP, and GM@BCP hydrogels; bone defects treated with GM@BCP hydrogels were significantly healed (Fig. 9a). H&E staining showed excessive number inflammatory cell in both control and GM groups, while other groups displayed only a few number of inflammatory cells (Fig. 9b). GM@CP and GM@BCP groups exhibited a more pronounced nascent calvarial thickness, thereby further indicating the beneficial effect of the CP to recruit calcium ions (Ca^{2+}) to induce mineralization *in vivo*. MT staining also demonstrated considerable bone healing rate in the GM@BCP group compared with the other groups. Meanwhile, there was no clear boundary between *de novo* bone and the native bone, thereby indicating that implanted hydrogels were fused with the surrounding bone tissue due in part to their favorable osseo-integration ability (Fig. 9c).

Based on the recruitment of endogenous VEGF to promote angiogenesis, IF staining for CD31 and α-SMA was carried out to discern neovascularization of newly formed bone tissues (Fig. 10). As shown in Fig. 10b, GM@BP and GM@BCP groups exhibited more positive area for CD31 and α-SMA than that of the other groups. It is worth to note that GM@BCP group exhibited less positive area of CD31 and α-SMA staining than that of the GM@BP group, which may be ascribed to the mature bone in the preceding group than the later and potential vascular degeneration (Fig. 10d and e). GM@BP, GM@CP, and GM@BCP groups also exhibited more expressions of OCN and OPN than that of the control and GM groups; GM@BP and GM@BCP groups performed better than that of the GM@CP in terms of osteoblast markers (Figs. 10c, 9f-9g).

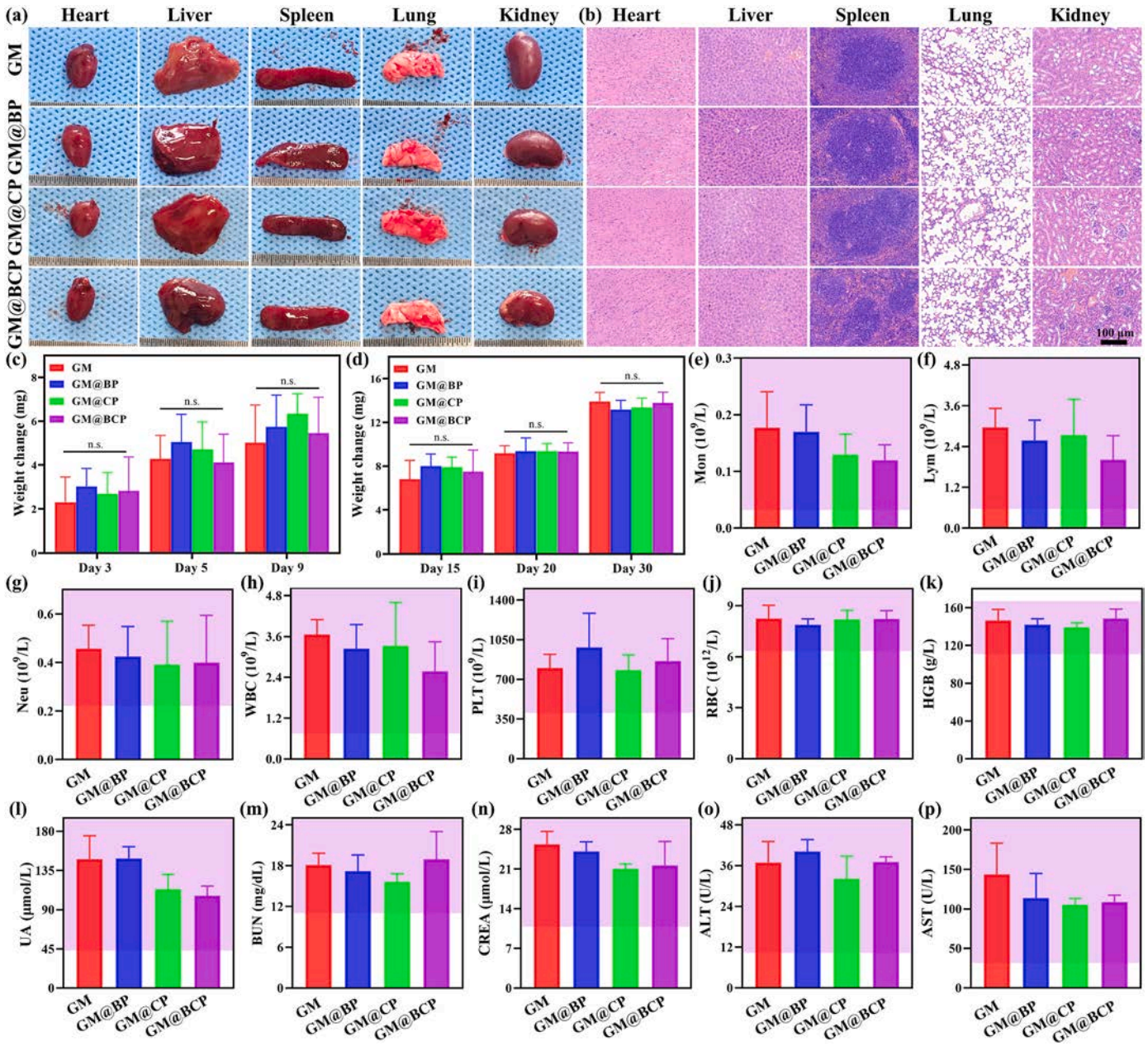

Fig. 8. Safety of subcutaneously implanted hydrogels in ICR rats. Appearance (a) and H&E staining (b) of main organs at day 30 of hydrogel implantation. The weight change in ICR rats for acute toxicity assessment (c) as well as medium- and long-term toxicity assessment (d). Number of migrated cells (e–j), HGB (k), and serum biochemical analysis (l–p) in the blood for GM, GM@BP, GM@CP, and GM@BCP groups.

Taken together, GM@BCP hydrogel could simultaneously induce angiogenesis and osteogenesis, as well as promote bone mineralization, which may have broad implications for bone tissue regeneration.

4. Discussion

In clinical practices, there are multifaceted factors, which can cause bone defects, such as trauma, osteoporosis, osteomyelitis, periodontitis, hereditary diseases, and so on [27]. These bone defects could disrupt physical integrity of the patient as well as impair normal physiological function. Different types of scaffolds with tunable physical and chemical properties (*e.g.,* shape, porosity, composition) and biofunctions (*e.g.,* biocompatibility, biodegradability, osteoconductivity) have been developed for bone defect healing [10,28]. Interestingly, the structure and composition of ATRS for bone defect repair should accommodate stem cells, stimulate cell attachment, cell proliferation, cell differentiation, and promote ECM deposition, which may have implications for the reconstruction of vascular networks, and connective tissue ingrowth for functional bone tissue repair [26].

Moreover, the bone, as an heterogenous composite tissue, harbors inorganic minerals, such as hydroxyapatite and Col-I [27]. Bone remodeling usually refers to bone matrix formation by osteoblasts and mineralization [27,29]. Bone defect repair involves distinct yet overlapping processes, including local inflammatory response, cartilage matrix degeneration, primary bone formation and bone remodeling [3]. Especially, neo-cartilage matrix is replaced with hard callus by endochondral ossification along with vascularization in the primary bone formation. On the other hand, the hard callus of the woven bone is remodeled into mature bone at the final stage [27]. Consequently, it is imperative to provide a microenvironment conducive to vascular regeneration and bone tissue mineralization.

Angiogenesis involves the concerted effect of different types of

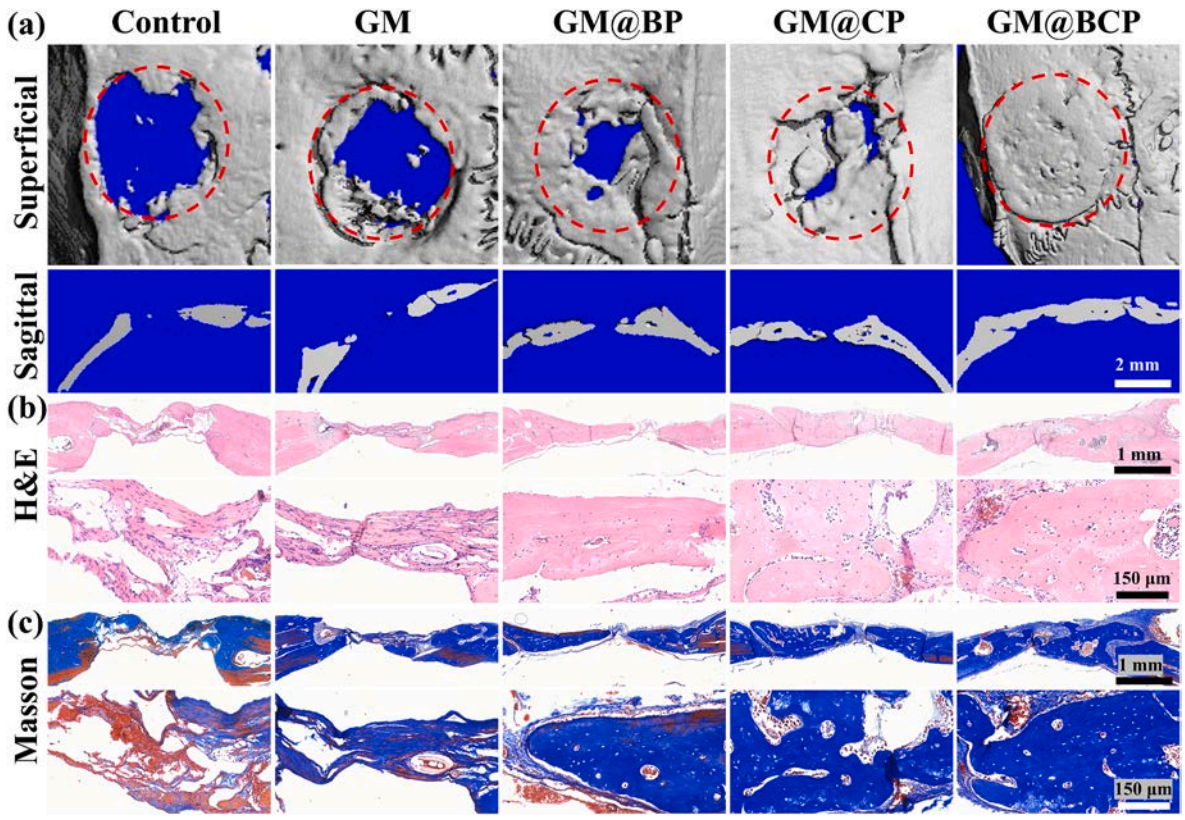

Fig. 9. The calvaria defect repair assay for 8 weeks *in vivo*. (a) 3D reconstructed micro-CT and sectioned graphs from tissue samples in defect site after hydrogel implantation for 8 weeks. The H&E staining (b) and MT staining (c) assay of hydrogel implantation in the defect site for 8 weeks post-implantation.

processes, including EC adhesion, proliferation, and migration [30]. Different types of approaches are used to induce vascularization, such as the incorporation of vasculogenic growth factors (GFs). Nevertheless, difficulties associated with the synthesis of large molecular weight proteins as well as well their inclusion into tissue-engineered scaffolds may limit their potential [13,31]. VEGF plays a pivotal role to stimulate the migration and proliferation of ECs. However, short half-life and poor retention of VEGF *in vitro* and *in vivo* may severly limit its application in tissue regeneration [32]. Recently, prominin-1-derived peptide, PR1P (DRVQRQTTTVVA) has been shown to facilitate soft tissue repair due in part to enhanced angiogenesis via improved VEGF binding and stabilization *in situ*. The BP can recruit endogenous VEGF by binding to its receptors, namely VEGFR1 and neuropilin-1, and promote cell viability and cell proliferation [26].

Therefore, BP can be incorporated into GM hydrogels to obtain GM@BP with various biological functions, *e.g.,* VEGF-mediated angiogenesis and immuno-modulation. However, GM@BP scaffold may still not be conducive for bone tissue repair due to various shortcomings, such as poor osteogenic mineralization and inferior mechanical properties [8]. To improve biomineralization, inorganic nanoparticles (NPs) with osteogenic abilities, including hydroxyapatite (HAP), bioactive glasss (BG), and silica (SiO_2) short fibers are widely used for bone tissue repair albeit their slower degradation *in vivo* and potential cytotoxicity at the injury site *in vivo* [33]. HAP ($Ca_{10}(PO_4)_6(OH)_2$) is an inorganic component of the bone tissues, which is formed by an electrostatic interaction between calcium ions (Ca^{2+}) and phosphate ions (PO_4^{3-}) [27,34].

The CP is a short peptide composed of five amino acids (PVAVT), which can bind calcium ions (Ca^{2+}) *in situ* to induce biomineralization [17]. Specially, functional binding sites of CP are an oxygen atom of the carboxylic (COOH) groups and a nitrogen atom of amino groups (-NH_2), thereby forming CP-Ca complex (Fig. 2b) [17]. Unlike most of the inorganic nanomaterials (NMs) as well as ceramic NPs, CP is a relatively simple bioactive molecule, which can be easily synthesized and incorporated into biomaterials. Moreover, CP can be easily metabolized by the body [22]. We observed enhanced mineralization of GM@BCP hydrogels in SBF *in vitro*, which is indicative of CP-mediated increase in the calcium ions (Ca^{2+}) binding and mineralization (Fig. 2c and d).

Bone tissue repair involves several overlapping phases, such as an inflammatory response, primary bone formation, and bone remodeling. While primary bone formation involves angiogenesis, bone remodeling involves mineralization [27,35]. Consequently, scaffolds for bone tissue repair should simultaneously induce osteogenesis and angiogenesis. Electrospun short fibers have been widely used to incorporate different types of biological and bioactive cues into 3D tissue-engineered scaffolds for both soft and hard tissue repair [21]. PLA/G short fibers are composed of a biocompatible and a biodegradable polymer 'PLA' and a natural polymer 'Gel' [36]. CP can therefore be loaded into PLA/G short fibers to obtain PLA/G@CP and co-formulated along with BP in GM to obtain GM@BCP hydrogels (Figs. 2f & 3b).

In GM@BCP hydrogels, the BP can be directly released from hydrogel, while CP needs to be first released from PLA/G short fibers into the hydrogels, and thereafter it can be released from hydrogel with a certain lag, thereby constructing a sequential release system (Fig. S10, Supporting Materials). The phased release of BP and CP from GM@BCP hydrogels can help achieve equential vascularization and mineralization for bone tissue repair. PLA/G@CP can prolong the degradation period of hydrogels at least for up to 12 weeks [23,37]. Moreover, PLA/G short fibers were uniformly dispersed into hydrogels. Since the degradation of GM is faster than that of the degradation of PLA/G fibers, the bulk matrix of hydrogels can degrade faster than that of the fibers for the rapid release of BP to promote vascularization. Therefore, the incorporation of PLA/Gel-based short fibers may prolong the degradation cycle of GM hydrogels.

Meanwhile, mechanical properties of hydrogels play a pivotal role for bone tissue repair, which may additionally influence cell

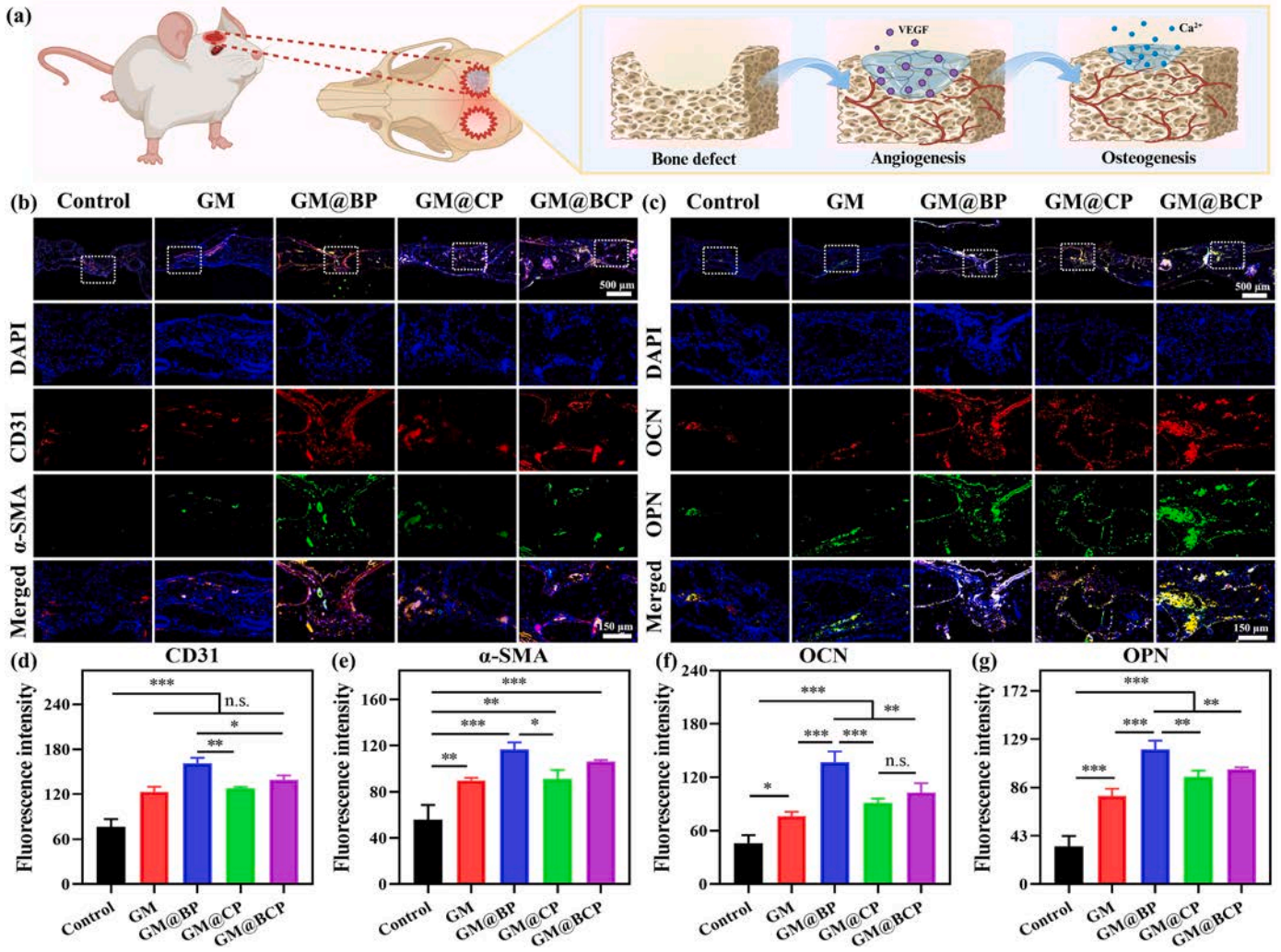

Fig. 10. IF staining of explants as well as bone surrounding tissues 8 weeks post-operatively. (a) Schematic representation of the recruitment of calcium ions (Ca^{2+}) and binding of VEGF *in situ*. IF staining for CD31 and α-SMA (b) as well as OCN and OPN (c) 8 weeks post-operatively. Quantitative analysis of positively stained areas of CD31 (d), α-SMA (e), OCN (f), and OPN (g) IF staining.

proliferation, cell differentiation, and matrix-mineral deposition via cell mechano-transduction [27]. Nonetheless, GM hydrogels may not accurately recapitulate the mechanical properties of native bone tissues (compressive strength: human cortical bone, 130–200 MPa and GM hydrogels, 0.02–0.2 MPa) [25,27]. PLA/G@CP short fiber may therefore improve mechanical properties of GM hydrogels (Fig. 3g–i). PLA/G@CP short fibers-mediated increase in the mechanical properties of hydrogels can be attributed to different aspects: *i*) GM hydrogel exhibits a certain degree of brittleness, thereby adversely influencing the mechanical properties [38]. *ii*) The incorporation of PLA/G@CP short fibers into GM hydrogels can pormote fiber-fiber and fiber-hydrogel interaction, thereby strengthening the mechanical properties of hydrogels. *iii*) Short fibers may also help form double-crosslinked network; the latter may additionally reinforce the mechanical properties of hydrogels [39]. Moreover, rough surface of the scaffold can promote an nteraction with the osteoblasts. PLA/G@CP short fiber can increase the roughness of GM hydrogels, thereby promoting an interaction with the osteoblasts (Fig. 3c) [27,40].

Scaffolds for bone tissue repair should also meet the general requisite to fit irregular-shaped defects and they should also be biocompatible, non-toxic, and bioresorbable [16,41]. GM@BCP hydrogel displayed considerable promise for the filling of irregular-shaped bone defects and additionally exhibited multiple advantegsous features, including significant tissue adhesion, cytocompatibility, cell migration, and angiogenesis *in vitro*. Moreover, GM@BCP hydrogels can degrade and promote ECM deposition *in vivo* (Fig. 4a–e, Fig. 7b). While initial acute inflammatory response may be important for the recruitment of osteo-progenitor cells as well as promote their osteo-genic induction, prolonged chronic inflammatory response may induce fibrosis and granuloma formation to hamper bone defect [42,43]. Tanscriptomics analysis revealed that the BP can modulate HUVECs, improve cell viability and cell proliferation, and reduce the expression of pro-inflammatory genes, which is indicative of the ability of the BP to support angiogenic function of HUVECs as well as resolve inflammatory response (Fig. 6e and f).

The BP could recruit endogenous VEGF to promote angiogenesis; neo-vessels can promote the diffusion of oxygen as well as increase the transport of nutrients (Fig. 10) [11,44]. Moreover, BP can upregulate ALP activity and Col-I secretion. On the other hand, CP can recruit calcium ions (Ca^{2+}) *in situ*, thereby inducing mineralization (Figs. 3f, 5b-5e). BP and CP upregulated the expression of OCN and OPN, which could collaboratively induce the deposition of calcium ions (Ca^{2+}) and phosphate ions (PO_4^{3-}) along with collagen fibers to obtain high quality bone ECM regeneration (Fig. 10b). Therefore, these characteristics and biofunction of GM@BCP hydrogels may have implications to promote bone tissue repair.

While different types of ceramics and tissue-engineered scaffolds with or without GFs have been used for bone tissue repair, such as HA/

tricalcium phosphate (HA/TCP) or HA/TCP along with recombinant BMP-2 (rhBMP2), GM@BCP scaffolds may have significant advantages as compared to the tradiational ceramics and tissue-engineered scaffolds. Bioactive glass (BG) can promote angiogenesis via the release of therapeutic ions [45]. On the other hand, BP can bind VEGF *in situ* for neovascularization, while CP can promote osteogenesis via enhanced recruitment of endogenous calcium ions (Ca^{2+}) *in situ*. Consequently, GM@BCP hydrogels may have higher biosafety for osteogenic mineralization of tissue-engineered scaffolds. An inclusion of CP in short fibers as well as encapsulation of these short fibers along with BP in GM hydrogels may help achieve sustained and controlled release of bioactive cues for concurrent osteogenesis and angiogenesis for bone tissue repair. Besides, the high concentration of therapeutic ions released from ceramics can pose potential toxicity risk [46].

Although GM@BCP hydrogels have shown significant potential for the regeneration of calverial defect, further evaluation is needed for the regeneration of irregular-shaped bone defects or critical-sized bone defects. In our previous study, we observed the repair of critical-sized tibial defect (length, 2 mm) with PRP-loaded GM hydrogels albeit poor bone healing performance for 4 mm bone defects 8 weeks post-operatively [8]. Therefore, it is imperative to further optimize the structure of GM@BCP hydrogels to accelerate the rate of tissue infiltration, especially, for the regeneration of large-size bone defects. Since GM hydrogels exhibit photo-crosslinking ability, regeneration of large-sized bone defects or irregular-shaped bone defects can be achieved through different molds or in-situ gelatinization.

However, this study has also several limitations. Firstly, hydrogels displayed certain degree of mechanical properties albeit further requirement for an improvement of the mechanical properties of hydrogels, especially, for the regeneration of load-bearing as well as large-sized bone defects. BP and CP were simultaneously used to promote the binding and stabilization of VEGF as well as the recruitment of calcium ions (Ca^{2+}) *in situ*, the relationship between BP and CP as well as a dose-dependent effect of peptides yet remains to be clarified. Secondly, we indirectly evaluated the release kinetics of BP and CP from GM@BCP hydrogels by incorporating Rhodamine and 5-FITC into hydrogels as representative molecules for the BP and CP, respectively, which may not accurately replicate the peptide and therefore can not provide a deep insight into the release kinetics of peptides from the GM@BCP hydrogels. Therefore, the incorporation of fluorescently-labelled peptides as well as their release kinetics should be performed in the subsequent studies. Thirdly, a rat calverial defect model was chosen to evaluate the potential of scaffolds to induce bone tissue repair. Since skull is a non-stressed bone, it may not accurately represent the bone defect model, especially, to delineate the ability of the scaffolds for the regeneration of large-sized bone defects or loead-bearing bone defects. Therefore, it is imperative to screen the ability of the scaffolds for the regeneratioin of alternative bone defect models, such as tibia. Nevertheless, we deciphered the ability of GM@BCP to achieve the sustained and controlled release of bioactive cues as well as influence the biological function for an effective bone tissue repair, which may increase our understanding of the biomaterials-mediated bone TE and potentially other related disciplines.

5. Conclusion

In this work, *in situ* injectable GM@BCP hydrogels loaded with BP and PLA/G@CP short fibers were prepared and used for bone tissue repair. The GM@BCP hydrogels were found to be cytocompatible, non-toxic, and bioresorbable, and were mostly degraded for up to 28 days *in vivo*. In the biofunction assay *in vitro*, BP could recruit VEGF *in situ* to promote angiogenesis, confer immunomodulatory potential and improve cell viability and proliferation. The CP can recruit calcium ions (Ca^{2+}) to accelerate osteogenic mineralization (quantitative ARS staining: 0.34 ± 0.05 and 1.06 ± 0.10 for GM and GM@CP hydrogels). Moreover, BP and CP upregulated OCN and OPN protein expression, which could collaboratively induce bone mineralization to obtain high quality bone ECM regeneration in a rat calvarial defect model *in vivo*. Taken together, our approach of the concurrent delievery of BP and CP from GM@BCP hydrogels may be worthy for future investigations aimed at bone tissue repair.

CRediT authorship contribution statement

Zhengchao Yuan: Writing – original draft, Software, Investigation, Conceptualization. **Xinyi Wang:** Validation, Formal analysis, Data curation. **Peng Li:** Visualization, Software, Funding acquisition. **Muhammad Shafiq:** Writing – review & editing, Writing – original draft, Validation, Supervision, Methodology, Funding acquisition, Formal analysis. **Panpan Shang:** Funding acquisition. **Lu Han:** Validation, Software, Methodology. **Hao Feng:** Visualization, Validation. **Yuan Xu:** Validation, Funding acquisition. **Mohamed El-Newehy:** Funding acquisition. **Meera Moydeen Abdulhameed:** Resources, Funding acquisition. **Lianyong Jiang:** Writing – review & editing, Supervision, Funding acquisition, Data curation. **Xiumei Mo:** Writing – review & editing, Supervision, Project administration, Funding acquisition, Data curation, Conceptualization. **Yijiu Ren:** Writing – review & editing, Visualization, Supervision, Project administration, Funding acquisition.

Declaration of competing interest

The authors declare that they have no known competing financial interests or personal relationships that could have appeared to influence the work reported in this paper.

Acknowledgments

This project was supported by the Fundamental Research Funds for the Central Universities and Graduate Student Innovation Fund of Donghua University (CUSF-DH-D-2024040), Natural Science Foundation of Shandong Province (grant number ZR2020QH071), Science and Technology Commission of Shanghai Municipality, China (20DZ2254900), Sino German Science Foundation Research Exchange Center, China (M − 0263), and China Education Association for International Exchange (2022181). This project was also supported by Researchers Supporting Project Number (RSP2025R65), King Saud University, Riyadh, Saudi Arabia. The authors would like to sincerely acknowledge the kind support of the Hangzhou KaiTai Bio-lab for whole transcriptome sequencing analysis and http://www.home-for-researchers.com with the help for the drawing of the schematic in Fig. 1.

Appendix A. Supplementary data

Supplementary data to this article can be found online at https://doi.org/10.1016/j.biomaterials.2025.123352.

Data availability

Data will be made available on request.

References

[1] A. Torres-Mansilla, M. Hincke, A. Voltes, E. López-Ruiz, P.A. Baldión, J.A. Marchal, P. Álvarez-Lloret, J. Gómez-Morales, Eggshell membrane as a biomaterial for bone regeneration, Polymers 15 (2023) 1342.
[2] Z. Fu, D. Li, J. Cui, H. Xu, C. Yuan, P. Wang, B. Zhao, K. Lin, Promoting bone regeneration via bioactive calcium silicate nanowires reinforced poly (ε-caprolactone) electrospun fibrous membranes, Mater. Des. 226 (2023) 111671.
[3] Z. Yuan, L. Zhang, M. Shafiq, X. Wang, P. Cai, A. Hafeez, Y. Ding, Z. Wang, M. Elnewehy, M. Moydeen, L. Jiang, X. Mo, Y. Xu, Composite superplastic aerogel scaffolds containing dopamine and bioactive glass-based fibers for skin and bone tissue regeneration, J. Colloid Interface Sci. 673 (2024) 411–425.

[4] L. Ouyang, B. Chen, X. Liu, D. Wang, Y. Li, Y. Liao, K.W.K. Yeung, X. Liu, Puerarin@Chitosan composite for infected bone repair through mimicking the bio-functions of antimicrobial peptides, Bioact. Mater. 21 (2023) 520–530.
[5] B. Zhao, Y. Zhang, D. Li, X. Mo, J. Pan, Hofmeister effect-enhanced gelatin/oxidized dextran hydrogels with improved mechanical properties and biocompatibility for wound healing, Acta Biomater. 151 (2022) 235–253.
[6] Z. Cai, Q. Saiding, L. Cheng, L. Zhang, Z. Wang, F. Wang, X. Chen, G. Chen, L. Deng, W. Cui, Capturing dynamic biological signals via bio-mimicking hydrogel for precise remodeling of soft tissue, Bioact. Mater. 6 (2021) 4506–4516.
[7] P. Cai, L. Cao, Y. Ding, Y. Han, X. Yu, J. Cui, H. Wang, J. Wu, M. EL-Newehy, M. M. Abdulhameed, X. Mo, S. Wang, B. Sun, Modified highly elastic 3D nanofiber embolic scaffolds for precise in situ embolization therapy, Adv. Funct. Mater. 34 (2024) 2316590.
[8] S. Lian, Z. Mu, Z. Yuan, M. Shafiq, X. Mo, W. Mu, Methacrylated gelatin and Platelet-rich plasma based hydrogels promote regeneration of critical-sized bone defects, Regen. Biomater. 11 (2024) rbae022.
[9] S. Li, Y. Sun, Y. Chen, J. Lu, G. Jiang, K. Yu, Y. Wu, Y. Mao, H. Jin, J. Luo, S. Dong, B. Hu, Y. Ding, A. Liu, Y. Shen, G. Feng, S. Yan, Y. He, R. Yan, Sandwich biomimetic scaffold based tendon stem/progenitor cell alignment in a 3D microenvironment for functional tendon regeneration, ACS Appl. Mater. Interfaces 15 (2023) 4652–4667.
[10] L. Qi, X. Fang, J. Yan, C. Pan, W. Ge, J. Wang, S.G. Shen, K. Lin, L. Zhang, Magnesium-containing bioceramics stimulate exosomal miR-196a-5p secretion to promote senescent osteogenesis through targeting Hoxa7/MAPK signaling axis, Bioact. Mater. 33 (2024) 14–29.
[11] Y.B. Rosanto, C.Y. Hasan, R. Rahardjo, T.W. Pangestiningsih, Effect of snail mucus on angiogenesis during wound healing, F1000Research 10 (2021) 181.
[12] Z. Yuan, D. Sheng, L. Jiang, M. Shafiq, A. ur R. Khan, R. Hashim, Y. Chen, B. Li, X. Xie, J. Chen, Y. Morsi, X. Mo, S. Chen, Vascular endothelial growth factor-capturing aligned electrospun polycaprolactone/gelatin nanofibers promote patellar ligament regeneration, Acta Biomater. 140 (2022) 233–246.
[13] A. Adini, H. Wu, D.T. Dao, V.H. Ko, L.J. Yu, A. Pan, M. Puder, S.Z. Mitiku, R. Potla, H. Chen, J.M. Rice, B.D. Matthews, PR1P stabilizes VEGF and upregulates its signaling to reduce elastase-induced murine emphysema, Am. J. Respir. Cell Mol. Biol. 63 (2020) 452–463.
[14] J. Zhou, R. Cha, Z. Wu, C. Zhang, Y. He, H. Zhang, K. Liu, M.S. Fareed, Z. Wang, C. Yang, Y. Zhang, W. Yan, K. Wang, An injectable, natural peptide hydrogel with potent antimicrobial activity and excellent wound healing-promoting effects, Nano Today 49 (2023) 101801.
[15] H. Liu, R. Gu, W. Li, L. Zeng, Y. Zhu, B.C. Heng, Y. Liu, Y. Zhou, Engineering 3D-printed strontium-titanium scaffold-integrated highly bioactive serum exosomes for critical bone defects by osteogenesis and angiogenesis, ACS Appl. Mater. Interfaces 15 (23) (2023) 27486–27501.
[16] J. Yang, C. Deng, M. Shafiq, Z. Li, Q. Zhang, H. Du, S. Li, X. Zhou, C. He, Localized delivery of FTY-720 from 3D printed cell-laden gelatin/silk fibroin composite scaffolds for enhanced vascularized bone regeneration, Smart Mater. Med. 3 (2022) 217–229.
[17] L. Wang, Y. Ding, X. Zhang, Y. Li, R. Wang, X. Luo, Y. Li, J. Li, Z. Chen, Isolation of a novel calcium-binding peptide from wheat germ protein hydrolysates and the prediction for its mechanism of combination, Food Chem. 239 (2018) 416–426.
[18] K. Zhang, J. Li, H. Hou, H. Zhang, B. Li, Purification and characterization of a novel calcium-biding decapeptide from Pacific cod (Gadus Macrocephalus) bone: molecular properties and calcium chelating modes, J. Funct.Foods 52 (2019) 670–679.
[19] Z. Yuan, Y. Zhao, M. Shafiq, J. Song, J. Hou, Y. Liang, X. Yu, Multi - functional fibrous dressings for burn injury treatment with pain and swelling relief and scarless wound healing, Adv. Fiber Mater. 5 (2023) 1963–1985.
[20] Y. Fang, C. Wang, Z. Liu, J. Ko, L. Chen, T. Zhang, Z. Xiong, L. Zhang, W. Sun, 3D printed conductive multiscale nerve guidance conduit with hierarchical fibers for peripheral nerve regeneration, Adv. Sci. 10 (2023) 2205744.
[21] X. Wang, Z. Yuan, M. Shafiq, G. Cai, Z. Lei, Y. Lu, X. Guan, R. Hashim, M. El-Newehy, M.M. Abdulhameed, X. Lu, Y. Xu, X. Mo, Composite aerogel scaffolds containing flexible silica nanofiber and tricalcium phosphate enable skin regeneration, ACS Appl. Mater. Interfaces 16 (2024) 25843–25855.
[22] W. Nie, E.J. Marrotte, R. Xie, H.G. Machens, A.F. Schilling, Y. Shen, M. Seeds, A. Atala, X. Dai, Towards scarless repair: MMP-2 responsive drug releasing nanofibrous mat restores homeostasis via fibroblasts' activation, Compos. Part B Eng. 291 (2025) 111972.
[23] Z. Yuan, Y. Ren, M. Shafiq, Y. Chen, H. Tang, B. Li, M. EL-Newehy, H. EL-Hamshary, Y. Morsi, H. Zheng, X. Mo, Converging 3D printing and electrospinning: effect of poly(L-lactide)/gelatin based short nanofibers aerogels on tracheal regeneration, Macromol. Biosci. 22 (2022) 2100342.
[24] Y. Xu, Q. Saiding, X. Zhou, J. Wang, W. Cui, X. Chen, Electrospun fiber-based immune engineering in regenerative medicine, Smart Med 3 (2024) e20230034.
[25] L. Zhang, Z. Yuan, M. Shafiq, Y. Cai, Z. Wang, P. Nie, X. Mo, Y. Xu, An injectable integration of autologous bioactive concentrated growth factor and gelatin methacrylate hydrogel with efficient growth factor release and 3D spatial structure for accelerated wound healing, Macromol. Biosci. 23 (2023) 2200500.
[26] Y. Chen, Z. Yuan, W. Sun, S. Muhammad, J. Zhu, J. Chen, H. Tang, Vascular endothelial growth factor - recruiting nanofiber bandages promote multifunctional skin regeneration via improved angiogenesis and immunomodulation, Adv. Fiber Mater. 5 (2023) 327–348.
[27] S.P. Malliappan, A.A. Yetisgin, S.B. Sahin, E. Demir, S. Cetinel, Bone tissue engineering: anionic polysaccharides as promising scaffolds, Carbohydr. Polym. 283 (2022) 119142.
[28] Z. Song, H. Yu, L. Hou, Y. Dong, M. Hu, P. Wei, W. Wang, D. Qian, S. Cao, Z. Zheng, Z. Xu, B. Zhao, Y. Huang, W. Jing, X. Zhang, Mechanics-resilient HA/SIS-based composite scaffolds with ROS-scavenging and bacteria-resistant capacity to address infected bone regeneration, Adv. Funct. Mater. 34 (2024) 2315382.
[29] X. Haixia, Z. Peng, L. Jiezhao, G. Huiling, C. Xie, W. Yihan, J. Yanglei, J. Li, C. Wang, X. Wenning, Z. Lixin, C. Liu, 3D-printed magnesium peroxide-incorporated scaffolds with sustained oxygen release and enhanced photothermal performance for osteosarcoma multimodal treatments, ACS Appl. Mater. Interfaces 16 (2024) 9626–9639.
[30] S. Tomar, R. Pandey, P. Surya, R. Verma, R. Mathur, G. Gangenahalli, S. Singh, Multifunctional, adhesive, and PDA-coated bioactive glass reinforced composite hydrogel for regenerative wound healing, ACS Biomater. Sci. Eng. 9 (2023) 1520–1540.
[31] Y. Han, J. Yang, W. Zhao, H. Wang, Y. Sun, Y. Chen, J. Luo, L. Deng, X. Xu, W. Cui, H. Zhang, Biomimetic injectable hydrogel microspheres with enhanced lubrication and controllable drug release for the treatment of osteoarthritis, Bioact. Mater. 6 (2021) 3596–3607.
[32] Z. Chen, N. Zhong, J. Wen, M. Jia, Y. Guo, Z. Shao, X. Zhao, Porous three-dimensional silk fibroin scaffolds for tracheal epithelial regeneration in vitro and in vivo, ACS Biomater. Sci. Eng. 4 (2018) 2977–2985.
[33] B. Pang, J. Xian, J. Chen, L. Ng, M. Li, G. Zhao, Y. E, X. Wang, X. Cao, C. Zhang, M. Zhang, C. Liu, Cuttlefish bone-derived calcium phosphate bioceramics have enhanced osteogenic properties, J. Funct. Biomater. 15 (2024) 212.
[34] X. Wang, M. Tang, Bioceramic materials with ion-mediated multifunctionality for wound healing, Smart Med 1 (2022) e20220032.
[35] P. Zhuang, W. Yang, Y. Chen, Y. Zhang, C. Leboucher, J.M. Rosenholm, H. Zhang, Biomaterials that passively and actively target macrophages promote the regeneration of injured tissues, Biomed. Technol. 8 (2024) 17–49.
[36] W. Chen, S. Chen, Y. Morsi, H. El-Hamshary, M. El-Newhy, C. Fan, X. Mo, Superabsorbent 3D scaffold based on electrospun nanofibers for cartilage tissue engineering, ACS Appl. Mater. Interfaces 8 (2016) 24415–24425.
[37] Y.J. Wei, H. Chen, Z.W. Zhou, C.X. Liu, C.X. Cai, J. Li, X.Q. Yu, J. Zhang, Y.H. Liu, N. Wang, Kill two birds with one stone: dual-metal MOF-nanozyme-decorated hydrogels with ROS-scavenging, oxygen-generating, and antibacterial abilities for accelerating infected diabetic wound healing, Small 20 (2024) 2403679.
[38] M. Wang, J. Du, M. Li, F. Pierini, X. Li, J. Yu, B. Ding, In situ forming double-crosslinked hydrogels with highly dispersed short fibers for the treatment of irregular wounds, Biomater. Sci. 11 (2023) 2383–2394.
[39] J. Lyu, Q. Zhou, H. Wang, Q. Xiao, Z. Qiang, X. Li, J. Wen, C. Ye, M. Zhu, Mechanically strong, freeze-resistant, and ionically conductive organohydrogels for flexible strain sensors and batteries, Adv. Sci. 10 (2023) 2206591.
[40] J. Wang, J. Lin, L. Chen, L. Deng, W. Cui, Endogenous electric-field-coupled electrospun short fiber via collecting wound exudation, Adv. Mater. 34 (2022) 2108325.
[41] C. Liu, X. Xu, W. Cui, H. Zhang, Metal-organic framework (MOF)-based biomaterials in bone tissue engineering, Eng. Regen. 2 (2021) 105–108.
[42] L.H. Wang, B.A. Marfil-Garza, A.U. Ernst, R.L. Pawlick, A.R. Pepper, K. Okada, B. Epel, N. Viswakarma, M. Kotecha, J.A. Flanders, A.K. Datta, H.J. Gao, Y.Z. You, M. Ma, A.M.J. Shapiro, Inflammation-induced subcutaneous neovascularization for the long-term survival of encapsulated islets without immunosuppression, Nat. Biomed. Eng. 8 (2023) 1266–1284.
[43] G. Zhu, R. Zhang, Q. Xie, P. Li, F. Wang, L. Wang, C. Li, Shish-kebab structure fiber with nano and micro diameter regulate macrophage polarization for anti-inflammatory and bone differentiation, Mater. Today Bio. 23 (2023) 100880.
[44] M. Schumacher, P. Habibović, S. Van Rijt, Peptide-modified nano-bioactive glass for targeted immobilization of native vEGF, ACS Appl. Mater. Interfaces 14 (2022) 4959–4968.
[45] Z. Yuan, S. Wu, L. Fu, M. Shafiq, Y. Liang, P. Li, X. Wang, H. Feng, R. Hashim, S. Lou, M. El-newehy, M. Moydeen, W. Zhang, X. Mo, S. Jiang, Composite scaffolds based on egg membrane and eggshell-derived inorganic particles promote soft and hard tissue repair, Compos. Part B. 292 (2025) 112071.
[46] X. Wang, Z. Yuan, G. Cai, Y. Lu, S. Zhou, P. Shang, C. Li, Z. Wang, Z. Liu, M. Shafiq, M. El-newehy, M.M. Abdulhameed, X. Lu, Y. Xu, X. Mo, Flexible short silica fibers and tricalcium phosphate synergistically promote bone fracture healing in composite cryogel scaffolds, Adv. Healthc. Mater. 14 (2025) 2404329.